

## Cold collisions of ground- and excited-state alkali-metal atoms

P. S. Julienne

*Molecular Physics Division, National Institute of Standards and Technology, Gaithersburg, Maryland 20899*

Jacques Vigué

*Laboratoire de Spectroscopie Hertzienne de l'Ecole Normale Supérieure, 24 Rue Lhomond, 75231 Paris, France*

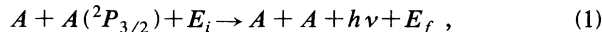
(Received 15 March 1991)

This paper examines two collisional mechanisms by which cold alkali-metal atoms can escape from a neutral-atom trap, due to collision of excited- and ground-state atoms. One is fine-structure-changing collisions, by which the atoms are heated by the amount of the fine-structure splitting. The other produces hot ground-state atoms following emission of a red-shifted photon during the course of a collision. A rate expression is obtained that applies to both normal and ultracold temperatures ( $< 1$  mK). This expression assumes a canonical distribution of initial states, low-intensity excitation, and a semiclassical treatment of the survival probability relative to excited-state decay during the long time of the ultracold collision, and uses fine-structure-changing probabilities found by quantum scattering calculations. The known properties of the attractive molecular states of the alkaline-metal dimers are used to identify and calculate the probabilities for the specific mechanisms. We conclude that the earlier semiclassical analysis by Dashevskaya [Opt. Spectrosk. **46**, 423 (1979)] of the fine-structure-changing mechanisms for the various alkali-metal species is qualitatively correct. We present quantum-mechanical calculations of the rate coefficient for fine-structure-changing collisions between ground- and excited-state Cs atoms from 1000 K to 100  $\mu$ K. Collision-rate coefficients for the trap-loss processes are calculated for pairs of Li, Na, K, Rb, and Cs atoms at low temperature. There is a wide variation of predicted loss rate among alkali-metal species from the fastest for K and the slowest for Li. Retardation corrections to molecular lifetimes must be taken into account to predict the correct rate coefficients for Na, K, and Rb. Good agreement is obtained with the observed trap loss rate in a Cs trap.

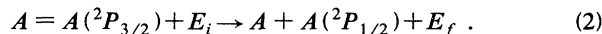
PACS number(s): 34.50.Rk, 34.50.Fa, 32.80.Pj

### I. INTRODUCTION

Recent advances in the laser cooling and trapping of neutral atoms make possible the confinement of alkali-metal atoms at ultracold temperatures,  $T < 1$  mK [1–15]. Collisional processes are expected to limit the density and time of confinement in such atom traps [16–23]. We proposed [16] and carried out calculations [19] on the rate of a radiative escape (RE) mechanism by which ultracold atoms in a neutral-atom trap can be lost from the trap:



where  $E_i$  and  $E_f$  are the kinetic energies in the respective initial and final states. This mechanism is a generic one which will apply to *any* laser-cooled atom, irrespective of whether or not it has fine or hyperfine structure. Gallagher and Pritchard [21] (GP) introduced an additional mechanism for alkali-metal atoms which involves a change of fine-structure (FS) level:



They developed a semiclassical model for calculating rate coefficients which gives qualitative agreement with the measured trap-loss rates in a Cs trap [22]. They also showed that the rate of the FS process is larger than the rate of the RE process for alkali-metal species.

In the RE mechanism the gain  $\Delta\epsilon$  in kinetic energy due to emission by the  $A_2$  molecule of a photon  $h\nu$ , which is red shifted from the atomic transition energy  $h\nu_A$ , is

$$\Delta E = E_f - E_i = h\nu_A - h\nu. \quad (3)$$

In the FS mechanism the kinetic energy gain is

$$\Delta E = E_f - E_i = \Delta E_{\text{FS}}, \quad (4)$$

where  $\Delta E_{\text{FS}}$  is the energy difference between fine-structure levels. If  $\Delta E$  is large enough, the hot product atoms will escape the weak trapping forces of a neutral atom trap and thereby be irreversibly lost from the trap. In a laser-cooling experiment an appreciable fraction of excited atoms will always be present if the cooling laser with energy  $h\nu_1$  is tuned slightly to the red of  $h\nu_A$ :

$$\delta = h\nu_A - h\nu_1 \approx h\gamma_A, \quad (5)$$

where  $\gamma_A$  is the linewidth (in Hz) of the atomic transition. We do not consider here the case where the detuning  $\delta$  is large compared to  $h\gamma_A$  so that bound states of the molecule are excited, nor do we consider the role of a second “catalysis” laser [22] at frequency  $\nu_2$ , where

$$h\nu_A - h\nu_2 \gg h\gamma_A. \quad (6)$$

The basic picture of the ultracold collision provided by the Gallagher and Pritchard paper [21] certainly captures

the essence of the novel physics of such collisions, and their semiclassical method provides a useful framework for describing these most interesting collisions. However, the GP theory made unnecessarily restrictive assumptions which miss important physical effects at low  $T$  and do not allow the theory to go correctly to the normal high- $T$  rate expressions as  $T$  increases. We relax these assumptions and show how to calculate the collision rates as a function of  $T$ . The production of the excited atom only occurs when the atoms are separated by a very large internuclear separation  $R$ , whereas the RE and FS mechanisms are molecular processes which only occur at much shorter  $R$ . Our generalizations are to introduce the role of relative angular momentum and of the known molecular states into both the long- and short-range physics. Rate coefficients for ultracold collisions can also be severely attenuated because the excited molecular state must survive relative to spontaneous emission during the collision as the atoms progress from the long-range zone where they are optically excited to the short-range zone of RE and FS transitions. We have discussed this effect in some detail elsewhere [19,23–27]. As GP did, we use a semiclassical treatment of this survival process, but show that it is necessary to include the effect of retardation on molecular decay rates.

We examine the molecular physics of RE and FS collisions for alkali atoms in order to address the following questions for low- $T$  collisions: (1) What are the basic physical mechanisms of these transitions and how do they vary among alkali-metal species? (2) How do the rate coefficients vary as a function of collision energy? We develop simple expressions for the rate of FS and RE collisional trap-loss processes which permit us to make estimates of the rate coefficients of trap loss for all alkali-metal species. We will identify a number of unresolved problems and hope to stimulate new research on the subject of collisions of ground- and excited-state alkali-metal atoms of the same species. We will first review the basic physics of ultracold collisions, and then derive the generalizations of the GP model. We will then review the basic molecular physics of alkali-metal dimers and describe the FS and RE processes at normal temperatures, including new calculations for the FS cross section in Cs. Then we will calculate the corrections due to excitation and survival at ultracold temperatures, and make predictions of the variation of trap-loss rate among alkali-metal species. We will conclude with suggestions for future research.

## II. THEORY OF LOW-TEMPERATURE COLLISION RATE COEFFICIENTS

### A. Laser cooling and trapping

A variety of experimental methods are available for the slowing and trapping of neutral atoms [2–15]. Two main characteristic temperatures appear in the laser-cooling process. One is the Doppler-cooling temperature  $T_D$  given by

$$k_B T_D = h \gamma_A / 2, \quad (7)$$

where  $k_B$  is the Boltzmann constant and the natural linewidth  $\gamma_A = 1/(2\pi\tau_A)$  is inversely proportional to the radiative lifetime  $\tau_A$  of the upper state of the cooling transition.  $T_D$  is 240  $\mu\text{K}$  for Na and 130  $\mu\text{K}$  for Cs. This already very low temperature can be achieved for atoms with a nondegenerate ground state, but in the general case, much lower temperatures can be achieved by polarization gradient cooling [28,29]. This other mechanism is limited to be a few times the other characteristic temperature, namely, the recoil temperature  $T_R$  given by

$$k_B T_R = \hbar^2 k_v^2 / 2m, \quad (8)$$

where  $k_v$  is the wave vector of the photon in resonance with the atomic transition and  $m$  is the atomic mass. At this temperature the atomic de Broglie wavelength is equal to the wavelength of light used for cooling. This limit is very low indeed:  $T_R = 2 \mu\text{K}$  for Na and 0.2  $\mu\text{K}$  for Cs. In an alkali optical confinement area the lowest temperatures reported have been  $\approx 10 \mu\text{K}$  for Na [11,12] and  $\approx 2 \mu\text{K}$  for Cs [14,15], but the density is not very high ( $\approx 10^8 \text{ cm}^{-3}$ ). In traps, higher densities up to  $10^{11} \text{ cm}^{-3}$  have been achieved, although often the temperatures are higher, on the order of 100  $\mu\text{K}$  or greater.

Laser-cooling methods can be applied in one dimension to slow a beam of atoms, in two dimensions to slow the transverse velocity components and brighten a beam, or in three dimensions to trap atoms. Although we will be primarily discussing collisions in traps here, we anticipate that longitudinal and transverse cooling will be applied to produce atomic beams with some degree of control over beam velocity [30]. We express the hope that single or crossed beam experiments may be possible in the future in which collisions can be studied at temperatures between the very cold temperatures  $< 1 \text{ mK}$  in current traps and the normal temperatures of conventional beam experiments. Therefore, it is important to have a theory of the temperature dependence of cold rate processes.

### B. Characteristics of ultracold collisions

Collisions in a trap irradiated by lasers typically involve excited states, since there will usually be a significant fraction of excited atoms. Consider first an atom with a ground  $S$  and excited  $P$  state. Collisions can involve  $S+S$ ,  $S+P$ , or  $P+P$ , and it is necessary to consider all such possibilities, although we concentrate here on the role of  $S+P$  collisions.

The long-range potentials are extremely important in ultracold collision dynamics. Neglecting for the moment retardation effects, the lead terms in the potentials for  $S+S$ ,  $S+P$ , and  $P+P$  are, respectively, the  $R^{-6}$  van der Waals term, the  $R^{-3}$  resonant dipole-dipole term, and the  $R^{-5}$  quadrupole-quadrupole term. (This neglects magnetic  $R^{-3}$  terms which are dominant only at very long range; see Sec. III A.) The longest range potential is clearly the  $R^{-3}$  potential for  $S+P$ , for which the potential is on the order of the natural linewidth, or  $2k_B T_D$ , near the characteristic distance

$$R_v = 1/k_v = \lambda_v / 2\pi, \quad (9)$$

which is about 1000 Å for alkali atoms. Since the atomic velocity at  $T_D$  is only 6 Å/ns for Na and 2 Å/ns for Cs, the internuclear distance  $R_A = v\tau_A$  traveled in an atomic lifetime  $\tau_A$  is much less than  $R_v$ . Therefore, the truly new feature of cold collisions is that the duration of the collision is considerably larger than the excited state lifetime. This introduces considerable complication in the description of such collisions.

During a collision involving two cold atoms in the presence of near-resonant laser light, the nearly stationary atoms can absorb and reemit many photons as they slowly approach one another at distances on the order of  $R_v$ . The quasimolecule does not remain in an asymptotically prepared state, but it is optically pumped. This may have important consequences if the ground state is degenerate. In this long-range region, the energies and the lifetime no longer have the free-atom values, but are affected by the molecular formation, including retardation effects. This quasimolecular optical pumping may perturb not only the internal state distribution, but also the velocity distribution of the two atoms with respect to the isolated atom distributions. Moreover, correlations between the states of the two atoms may be induced by optical pumping. We regard this problem of describing the long-range approach of the cold atoms as a fundamental unsolved problem, which is being addressed in a preliminary manner by several groups [31–33].

It is therefore convenient to divide an ultracold collision into three characteristic zones of distinct physical behavior. We designate these the outer, intermediate, and inner zones. The quasimolecular optical pumping which leads to the “preparation” of the two atoms for the collision occurs in the outer zone. The boundary between the outer and intermediate zones is by no means sharp, but should be regarded as occurring near  $R_v$ . The intermediate zone is described by almost conventional collision physics. It extends from  $R \approx R_v$  to the short-range distances where exchange overlap effects become important. Optical pumping can continue in the outermost part of this zone. As the atoms come together, the detuning introduced by the molecular interactions causes the molecules to no longer be in resonance with the laser tuned near the atomic transition. Since the molecule can no longer be efficiently excited, the excited-state population will typically decay by spontaneous emission before reaching the inner part of this intermediate zone. Such loss can suppress strongly the scattering flux in the excited channel and lead to greatly reduced effective cross sections [19,21–25]. However, we show below that it is possible to excite at  $R \approx R_v$  a molecular state which becomes metastable at short internuclear distances so that the state does not have significant radiative loss. The third and innermost zone, extending to a few tens of  $a_0$ , is characterized by strong molecular interactions. In this zone curve crossings and nonadiabatic interactions cause inelastic energy-transfer processes.

It is evident that the long time and distance scales of ultracold collisions introduce novel behavior into such collisions. In fact it is not clear that it is appropriate to describe such collisions by a conventional rate coefficient,

because of the nonconservative, or dissipative, part of the effective Hamiltonian introduced by spontaneous emission over the time scale of the collision [23]. In the outer zone the normal assumption of collision theory is violated that the atoms be “prepared” at  $t = -\infty$  independently of the collision. For ultracold collisions the “preparation” cannot be separated from the “collision,” which is no longer described by a conservative Hamiltonian, but by a dissipative one. The optical pumping at large  $R$  should be described by density-matrix methods (optical Bloch equations) which treat spontaneous emission in a natural way [23]. Indeed, at very large  $R$  the theory must reduce to the density-matrix description of laser cooling of isolated, independent atoms [28,29]. On the other hand, the collision in the inner zone is most naturally described by quantum-wave-function methods, which readily treat the multiple trajectories on different molecular potentials, but do not address the problem of optical pumping and spontaneous emission.

Our approach tries to give a simple description of what occurs in each of the three zones described above, thereby enabling us to define an effective rate coefficient for the overall process: (1) Optical pumping in the outer zone is not treated. We assume that the pair distribution function is simply the canonical distribution of incoming pairs at the initial temperature. (2) The excitation at large  $R$  of each molecular state is described by spherically averaged absorption cross sections, a procedure valid at low laser intensity. (3) Propagation in the intermediate region is treated semiclassically. The radiative losses are calculated for each molecular state by numerical integration of the decay along the trajectory, giving a survival factor which depends on the molecular state. Emission in the wing of the line, responsible for the RE process, is also treated semiclassically. (4) In the inner zone the nonadiabatic transition probabilities are found by a close-coupling wave-function calculation, using the best knowledge of the molecular states and their couplings. In describing (1)–(3) above, we ignore the splittings caused by hyperfine structure and light shifts. We also assume adiabatic motion on the body-fixed molecular states in the outer region where excitation occurs, and do not treat the nonadiabatic dynamics associated with the dynamical frame transformation between space- and body-fixed reference frames of electronic angular momentum quantization.

The strongest set of assumptions made by this kind of model are clearly those associated with the long-range physics. We ignore the correlations and velocity changes induced by the long-range optical pumping of the real atoms with hyperfine structure. GP made a similar set of assumptions, but applied them in an oversimplified manner that misses important physical effects (see Sec. III B, IV B, and IV C). The basic question we address here is the energy variation of the effective rate coefficients from the normal to the ultracold regime. This question was not addressed by GP. In fact, their formula leads to an incorrect high-temperature limit, since they did not treat the effect of relative angular momentum  $l$  on the collision. The improvements we

make in the GP theory are twofold: to incorporate the role of  $l$  and to use the real physics of the actual molecular states instead of a single “effective” state with averaged properties. The former improvement applies to assumptions (1), (3), and (4) of the previous paragraph, whereas the latter applies to (2), (3), and (4).

### C. High-temperature rate expressions

Before describing ultracold modifications to rate coefficients, we will first give the normal high-temperature expressions. In the molecular adiabatic picture, the cross section for a given adiabatic channel  $\beta$  is

$$\sigma(E, \beta) = (\pi/k^2) \sum_{l=0}^{\infty} (2l+1) P(E, l, \beta), \quad (10)$$

where the entrance channel kinetic energy is  $E = \hbar^2 k^2 / 2\mu$ ,  $\mu$  is the reduced mass, and the quantum probability of the process of interest for relative angular momentum  $l$  is  $P(E, l, \beta)$ . The quantum number  $l$  is related to the classical impact parameter  $b$  by

$$b = (l + \frac{1}{2}) / k. \quad (11)$$

Using (11) to change the summation over  $l$  in (10) to an integration over  $b$ , the corresponding semiclassical expression for the cross section is

$$\sigma^{\text{SC}}(E, \beta) = 2\pi \int_0^{\infty} b P(E, b, \beta) db. \quad (12)$$

We have shown that for collisions dominated by the  $R^{-3}$  resonant dipole-dipole interaction, a semiclassical treatment of the near-threshold collision dynamics should be valid as long as  $T \gg T_R$  [19,23].

Instead of cross section, we prefer to use the rate coefficient  $K(E, \beta)$ :

$$K(E, \beta) = \sigma(E, \beta) v, \quad (13)$$

where  $v$  is the relative collision velocity. In a cell with a statistical distribution of Zeeman sublevels, the observed rate coefficient for the ground- plus excited-state collision is the average of the coefficients for the  $2g_1 g_2$  asymptotic channels,

$$K(T) = \frac{1}{2g_1 g_2} \sum_{\beta} \langle \sigma(E, \beta) v \rangle, \quad (14)$$

where the brackets  $\langle \rangle$  imply a thermal average, and  $g_1, g_2$  are the respective ground- and excited-state atomic degeneracies. For our case of  $^2S_{1/2} + ^2P_{3/2}$ ,  $2g_1 g_2 = 16$  [34]. Note that  $\beta = 1, \dots, 16$  labels a nondegenerate molecular state component. For states with molecular angular momentum projection  $\Omega \neq 0$ , the molecular degeneracy is 2, and *both* components must be included in the sum.

The reaction probability will always decrease when  $l$  is larger than some characteristic  $l_{\text{max}}$ . In the present case, if  $T > 5T_D$  (see below), the cutoff for a given channel is due to the presence of a barrier in the excited-state entrance channel potential due to the competition between the attractive  $C_3(\beta)/R^3$  potential and the repulsive  $\hbar^2 l(l+1)/2\mu R^2$  centrifugal potential. The barrier for

channel  $\beta$  occurs at

$$R_C(E, \beta) = [C_3(\beta)/2E]^{1/3}, \quad (15)$$

and the cutoff is at

$$b_{\text{max}}(E, \beta) = l_{\text{max}}(E, \beta) / k = \sqrt{3} R_C(E, \beta). \quad (16)$$

The channel rate coefficient can be written as

$$K(E, \beta) = K_C(E, \beta) \overline{P(E, \beta)}, \quad (17)$$

where

$$K_C(E, \beta) = 3\pi \frac{C_3(\beta)^{2/3}}{\mu^{1/2} (2E)^{1/6}} \quad (18)$$

is the familiar Langevin capture rate coefficient for a  $R^{-3}$  long-range potential associated with capture cross section  $\pi b_{\text{max}}^2$ , and  $\overline{P}$  is the average probability of reaction

$$\overline{P(E, \beta)} = \frac{\sum_{l=0}^{l_{\text{max}}} (2l+1) P(E, l, \beta)}{\sum_{l=0}^{l_{\text{max}}} (2l+1)}. \quad (19)$$

In a thermal average  $(2E)^{-1/6}$  in (18) is replaced by

$$2/\pi \frac{\Gamma(\frac{4}{3})}{(2k_B T)^{1/6}} = \frac{1.00762}{(2k_B T)^{1/6}}, \quad (20)$$

and  $\overline{P(E, \beta)}$  is replaced by the thermal average  $\overline{P(T, \beta)}$ .

### D. Low-temperature modification of collision-rate coefficients

Let us now formulate the low-temperature rate expressions. GP introduced the number of pairs between  $R$  and  $R + dR$  and assumed all pairs react with equal probability and survival factors. This assumption fails as  $T$  is increased, since only pairs in the right  $l$  range can react and survival depends strongly on the initial kinetic energy  $E$ . Our generalization is to introduce the number of ground-state pairs per unit volume between  $R$  and  $R + dR$  which approach each other with energy between  $E$  and  $E + dE$  and with angular momentum  $l$ ,

$$dN(R, E, l) = \frac{N^2}{2} \frac{(2l+1) e^{-E/k_B T}}{h v(R, E, l) Q_{\text{tr}}} dR dE, \quad (21)$$

where  $Q_{\text{tr}} = (2\pi\mu k_B T/h^2)^{3/2}$  is the translational partition function per unit volume. The ground-state potential has been assumed to be a constant equal to zero in the long-range excitation region. The derivation of (21) is outlined in Appendix A. Each pair is excited to state  $\beta$  at the weak-field excitation rate  $\sigma(R, \beta)\phi$ , where  $\phi$  is the laser flux, and the mean photoabsorption cross section  $\bar{\sigma}$ , averaged over the  $g_1^2$  ground-state components, is derived in Appendix B:

$$\overline{\sigma(R, \beta)} = \frac{\lambda_v^2}{2\pi} \frac{1}{g_1^2} \left[ 1 + \left[ \frac{2\delta(R)}{h\gamma_{\beta}(R)} \right]^2 \right]^{-1} \quad (22a)$$

$$= \frac{\lambda_v^2}{2\pi} \frac{1}{g_1^2} \epsilon(R, \beta). \quad (22b)$$

Here  $\delta(R)$  is the  $R$ -dependent detuning  $\delta - C_3(\beta)/R^3$  for

state  $\beta$  with spontaneous decay rate  $2\pi\gamma_\beta(R)$ , where  $\delta$  is given by Eq. (5), and

$$\epsilon(R, \beta) = \frac{(h\gamma_\beta/2)^2}{(h\gamma_\beta/2)^2 + \delta(R)^2} \quad (23)$$

is the line-shape function introduced by GP, normalized to unity at  $\delta(R)=0$ .

The number of excitations to state  $\beta$  per unit time per unit volume is  $\sigma(R, \beta)\phi dN(R, E, l)$ . The number of reactions per unit time per unit volume is found by multiplying by the probability  $S(R, E, l, \beta)$  of survival on the excited state to short distance and the probability  $P(E, l, \beta)$  of short-range reaction, and then summing over all states  $\beta$  and angular momenta  $l$  and integrating over all distances  $R$  and energies  $E$ :

$$R(T) = \sum_{\beta} \sum_l \int P(E, l, \beta) \times S(R, E, l, \beta) \overline{\sigma(R, \beta)} \phi dN(R, E, l) . \quad (24)$$

The survival probability is

$$S(R, E, l, \beta) = \exp \left[ - \int_{t(R)}^{t(0)} 2\pi\gamma_\beta(t') dt' \right] , \quad (25)$$

where the time integral is over the classical path from excitation at distance  $R$  at time  $t(R)$  until reaction at time  $t(0)$  in the inner zone. Since the attractive potential strongly accelerates the approaching atoms, the fast short-range part of the path makes a negligible contribution to the integral in (25) and  $S$  is independent of the actual location of the crossing points that lead to reaction. Thus,  $t(0)$  is taken to be the time to reach the inner turning point.

After introducing (21) and (22) into (24), the reaction rate can be rewritten either in terms of an effective rate coefficient  $K_g(T)$  for ground-state collisions or an effective rate coefficient  $K^*(T)$  for ground-plus excited-state collisions:

$$R(T) = K_g(T) N^2 = K^*(T) N N^* , \quad (26)$$

where

$$K_g(T) = (g_2/g_1)(\lambda^2/2\pi)\phi\tau_A \epsilon_A K^*(T) \quad (27)$$

and

$$K^*(T) = \frac{1}{2g_1g_2} \sum_{\beta} \langle K(E, \beta) I(E, \beta) \rangle , \quad (28)$$

and  $K(E, \beta)$  is given by (17). In deriving (27) the low-power relation between  $N^*$  and  $N$  is assumed:

$$N^* = (g_2/g_1)(\lambda^2/2\pi)\phi\tau_A \epsilon_A N . \quad (29)$$

All effects due to excitation and spontaneous emission are included in the integral,

$$I(E, \beta) = \epsilon_A^{-1} \int_0^\infty \epsilon(R, \beta) \overline{S(R, E, \beta)} dR / \tau_A v , \quad (30)$$

where

$$\epsilon_A = [1 + (2\delta/h\gamma_A)^2]^{-1} \quad (31)$$

is the atomic line-shape factor and  $\bar{S}$  is found by averaging

the survival factor  $S(R, E, l, \beta)$  over angular momentum  $l$  weighted by  $P(E, l, \beta)$  and  $v/v(R, E, l)$  [see Eq. (21) above]:

$$\overline{S(R, E, \beta)} = \frac{\sum_{l'} (2l'+1) S(R, E, l', \beta) P(E, l', \beta) v/v(R, E, l')}{\sum_l (2l+1) P(E, l, \beta)} . \quad (32)$$

Note carefully that the cutoff in the  $l$  sum need not be the same in the numerator and denominator in (32). This is indicated by the  $l'$  index in the numerator. The cutoff in the denominator is due to the excited state centrifugal exclusion, and is defined to be the same  $l_{\max}$  as Eq. (16). The cutoff in the numerator is the same  $l_{\max}$  at high  $T$ , but if  $E$  is low enough the cutoff  $l_{\max, g}$  is due to centrifugal exclusion in the ground state, since  $l_{\max, g} < l_{\max}$ . We can make a simple estimate of when the ground-state exclusion applies by evaluating  $l_{\max, g}$  at the point  $R_x = [C_3(\beta)/\delta]^{1/3}$ , where the quasimolecule is in resonance with the light with detuning  $\delta$  from atomic resonance. Since the ground-state electronic potential is flat, setting  $E$  equal to the centrifugal potential at  $R_x$  gives

$$l_{\max, g}/k = \sqrt{3} [C_3(\beta)/\delta]^{2/3} . \quad (33)$$

Direct comparison of (33) and (15) and (16) shows that

$$l_{\max, g} < l_{\max} \quad \text{if } E < (3^{3/2}/2)\delta \approx 2.6\delta . \quad (34)$$

If  $\delta/h$  is one natural linewidth, Eqs. (34) and (7) show that the ground-state cutoff applies to the numerator in (32) if  $T < 5T_D$ , or about 1 mK for alkali species. Above 1 mK the cutoffs in the sums in the numerator and denominator are the same, namely,  $l_{\max}$  determined by the excited-state centrifugal exclusion.

This careful attention to the cutoffs to the sums in (32) is important, since it allows us to reduce (28) to limiting expressions in two cases, namely, the normal high-temperature expression, Eq. (14), and the special low-temperature expression of GP if their assumptions are introduced. First assume the temperature is large compared to the characteristic temperature  $T_S$ , at which atoms moving with relative kinetic energy  $E = k_B T_S$  travel  $R_v$  in one atomic lifetime  $\tau_A$ . When  $T \gg T_S$  the distance traveled in one lifetime,  $R_A = \tau_A v$ , is large compared to  $R_v$ , and the integral in (25) is dominated by the long-range part of the trajectory, where  $v(R, E, l) = v$ ,  $\epsilon(R, \beta) = \epsilon_A$ , and  $\tau(\beta) = \tau_A$  are constants independent of  $R$  and  $\beta$ . Then  $S(R, E, l, \beta) = \exp(-R/R_A)$ , and the integral in (30) approaches unity:

$$I(E, \beta) \rightarrow 1 \quad \text{when } E \gg k_B T_S . \quad (35)$$

In this limit, the effective excited-state rate coefficient  $K^*(T)$  in Eq. (28) approaches the conventional expression in Eq. (14). The nominal order of magnitude of  $T_S$  for alkali collisions is in the range 10–100 mK.

Let us now show how the expression of GP is obtained when their assumptions are introduced. If we assume

that  $P$  and  $S$  in (24) are independent of  $l$  and that  $P$  is independent of  $E$ , having respective values  $P_{\text{GP}}(\beta)$  and  $S_{\text{GP}}(R, E, \beta)$ , then simple algebra shows that the rate  $R(T)$  in (24) can be written as in (26) with

$$K_{\text{GP}}^* = \frac{1}{2\tau_A} \frac{1}{2g_1g_2} \sum_{\beta} \langle I_{\text{GP}}(E, \beta) P_{\text{GP}}(\beta) \rangle, \quad (36)$$

where

$$I_{\text{GP}}(E, \beta) = \epsilon_A^{-1} \int_0^{\infty} 4\pi R^2 \epsilon(R, \beta) S_{\text{GP}}(R, E, \beta) dR. \quad (37)$$

In order to obtain the GP expression (37), Eqs. (A7) and (A11b) in Appendix A are used to carry out the sum in the numerator of (32), subject to the low-temperature cutoff at  $l_{\text{max},g}$ . In addition, GP made an even more restrictive assumption that (36) could be evaluated using only a single “effective” attractive state, here denoted  $\beta = \text{eff}$ , so that  $g_1 = g_2 = 1$ . Also, the thermal average in (36) was replaced by evaluation of  $S_{\text{GP}}$  using an empirical correction to the time integral in (25) calculated assuming zero initial velocity after excitation. We find their correction to be valid if  $T$  is in the vicinity of 200–300  $\mu\text{K}$ , where the specific temperature depends on the alkali-metal species. But their Eq. (4), which gives the correction, contains a typographical error: the correction factor of 1.4 should be in the denominator, not the numerator. With these assumptions their Eq. (9) is obtained:

$$K_{\text{GP}}^* = \frac{1}{2\tau_A} \frac{1}{2} I_{\text{GP}}(\text{eff}) P_{\text{GP}}(\text{eff}), \quad (38)$$

where  $S_{\text{GP}}$  in (37) is evaluated using the rotationless potential of the “effective” state. The extra factor of 2 in the denominator of (38) should appear in Eq. (9) of GP if  $P_{\text{GP}}(\text{eff})$  is interpreted as the average probability of reaction, averaged over the eight attractive channels [if  $P_{\text{GP}}$  were interpreted as the probability averaged over all 16 entrance channels, attractive and repulsive, the factor of  $\frac{1}{2}$  in (38) would be missing]. We do not recommend using Eq. (38), since the restrictive assumptions miss important physical effects which affect these collisions. In particular, we show below that it is seriously wrong to use a single effective state with “average” properties and that  $P$  and  $S$  show strong dependence on  $l$ . The correct expressions (28) and (30) are almost as simple to evaluate numerically as (38), and these expressions permit an accurate evaluation of the physics of the collision in the intermediate- and short-range zones, as well as yielding the temperature dependence.

### III. MOLECULAR PHYSICS OF ALKALI-METAL DIMERS

#### A. Potential-energy curves

The molecular electronic states which correlate asymptotically at large  $R$  with  $S+S$  and  $S+P$  alkali-metal atomic states are well known [35–50]. Retardation effects on the molecular potentials and lifetimes occur when  $R$  is comparable to or larger than the critical distance  $R_v$  in Eq. (9) [36–38,40]. Assume for the moment that  $R < R_v$ , so we can work with the usual molecular adi-

abatic states quantized in a molecule fixed frame. We ignore splittings due to hyperfine structure, spin-spin interactions, and external optical or magnetic fields.

The ground-state atoms give rise to the chemically bound  $^1\Sigma_g^+$  ground state and to the repulsive  $^3\Sigma_u^+$  state with a shallow van der Waals well. Both states have identical long-range  $-C_6/R^6$  interaction potentials, which have a magnitude  $< 1$  mK for  $R > 89a_0$  for Na and  $R > 115a_0$  for Cs; at larger internuclear separations, the ground-state potential is essentially flat. Meath [39] showed that the actual long-range form when relativistic spin-spin interactions are taken into account is on the order of  $\alpha^2/R^3$ , where  $\alpha$  is the fine-structure constant, due to the long-range spin dipole-spin dipole coupling between the two electrons. At long range this relativistic term equals the van der Waals term at about  $300a_0$  for Na and  $500a_0$  for Cs. At these large distances, the mag-

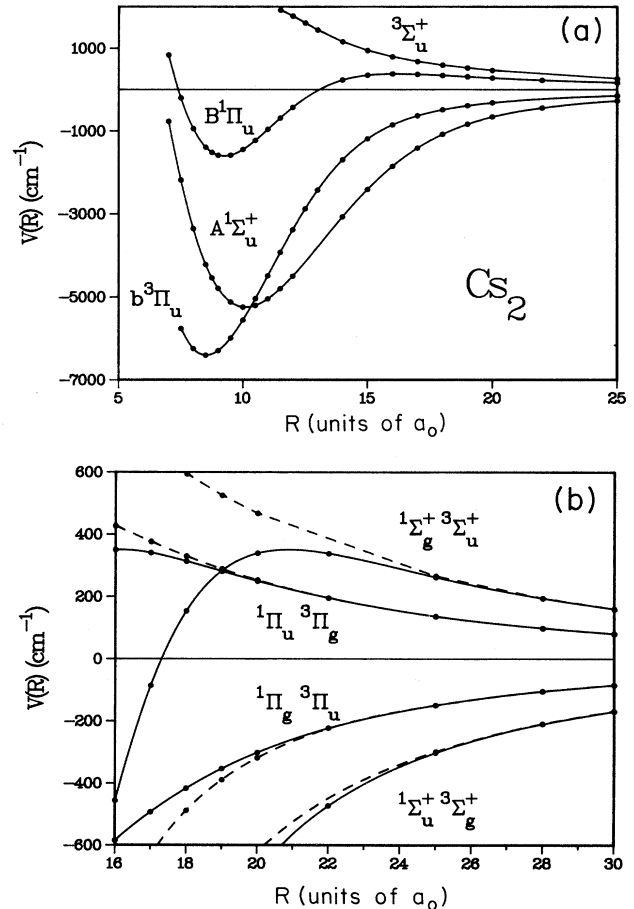


FIG. 1. (a) Nonrelativistic potential-energy curves for  $\text{Cs}_2$  calculated by Krauss and Stevens (Ref. [47]). Internuclear distance  $R$  is in atomic units,  $1a_0 = 0.529177 \times 10^{-8}$  cm. The solid circles show the calculated points. Hund’s case-(a) molecular symmetry labels are shown. (b) Nonrelativistic long-range potential-energy curves for  $\text{Cs}_2$  calculated by Krauss and Stevens.

TABLE I. Parameters of attractive states from  ${}^2P_{3/2} + {}^2S_{1/2}$  when  $C_3(\beta)/R^3 \ll \Delta E_{FS}$ .

| State $\beta$ | $C_3(\beta)^a$            | $\tau_{0,\beta}^b$             | $a_{0,\beta}$ | $a_{2,\beta}$   | $a_{4,\beta}$    |
|---------------|---------------------------|--------------------------------|---------------|-----------------|------------------|
| $0_u^+$       | $(\frac{5}{3})d^2$        | $(\frac{3}{4})\tau_A$          | $\frac{4}{3}$ | 0               | $-\frac{1}{840}$ |
| $1_g$         | $\frac{\sqrt{7}+2}{3}d^2$ | $\frac{21}{28-\sqrt{7}}\tau_A$ | 1.207 345     | 0.017 053       | -0.001 959       |
| $0_g^-$       | $d^2$                     | $(\frac{1}{2})\tau_A$          | 2             | $-\frac{2}{15}$ | $\frac{1}{168}$  |
| $1_u$         | $\frac{\sqrt{7}-2}{3}d^2$ | $\frac{21}{14-\sqrt{7}}\tau_A$ | 0.540 678     | 0.083 729       | -0.004 340       |
| $2_u$         | $d^2$                     | $\infty$                       | 0             | $\frac{1}{5}$   | $-\frac{3}{280}$ |

<sup>a</sup> $C_3$  is in atomic units,  $e^2a_0^2$ , and  $d = \langle {}^2S | d_z | {}^2P \rangle$  is in atomic units,  $ea_0$ .

<sup>b</sup> $\tau_{0,\beta}$  is the nonretarded molecular lifetime at long range.

nitude of the potential is  $< 1 \mu\text{K}$ , the potential is dynamically unimportant, and we are justified in ignoring this term as long as  $T \gg 1 \mu\text{K}$ .

The nonrelativistic potential curves which correlate with the  $P+S$  separated atom asymptotes are qualitatively similar for all the homonuclear alkali-metal dimers [41–47]. These are illustrated in Figs. 1(a) and 1(b), which show very accurate new curves obtained by Krauss and Stevens [47] using effective core potentials (ECP). Figure 1(b) shows that the long-range potential, dominated by the lead  $1/R^3$  term, applies to distances on the order of  $25a_0$ , inside of which exchange-overlap interactions give rise to chemical bonding effects as  $R$  decreases. Figure 1(a) shows the excited  $u$  (ungerade) potentials, for which the crossing of the  $A^1\Sigma_u^+$  and  $b^3\Pi_u$  states gives the dominant mechanism for the FS transition in Cs. A similar crossing occurs in all alkali-metal dimer pairs.

By diagonalizing the Hamiltonian matrix which includes the long-range nonrelativistic potentials and the relativistic spin-orbit coupling terms, the long-range potentials can be generated which correlate with the specific  ${}^2P_j + {}^2S_{1/2}$  fine-structure states [48–50]. These states are designated by their angular momentum projection  $\Omega$  on the molecular axis and their electronic inversion symmetry,  $g$  or  $u$ . There are four  $g$  and four  $u$  states (counting double degeneracies) correlating with the  ${}^2P_{1/2}$  asymptote and eight  $g$  and eight  $u$  states correlating with the  ${}^2P_{3/2}$  asymptote. Figures 2(a) and 2(b) illustrate the adiabatic (fully diagonalized)  $u$  potentials for  $\text{Cs}_2$  for  $e$  molecular parity,  $(-1)^J$ , for total angular momentum  $J=2$ . Only states having the same molecular parity classification,  $e$  or  $f$  [51–53], and the same  $J$  can mix with one another in a collision unperturbed by external fields.

There are four attractive molecular potentials which correlate with the  ${}^2P_{3/2}$  asymptote and have allowed dipole transitions connecting them to one of the ground-state potentials. The  $2_u$  state is also attractive, but is not optically coupled to the ground state if retardation is ignored. The total statistical weight of these attractive states is 8. These are the only states through which the FS or RE process can occur at low  $T$ . When  $R > R_v$ , retardation effects are known to lead to changes in the long-range potentials and molecular lifetimes

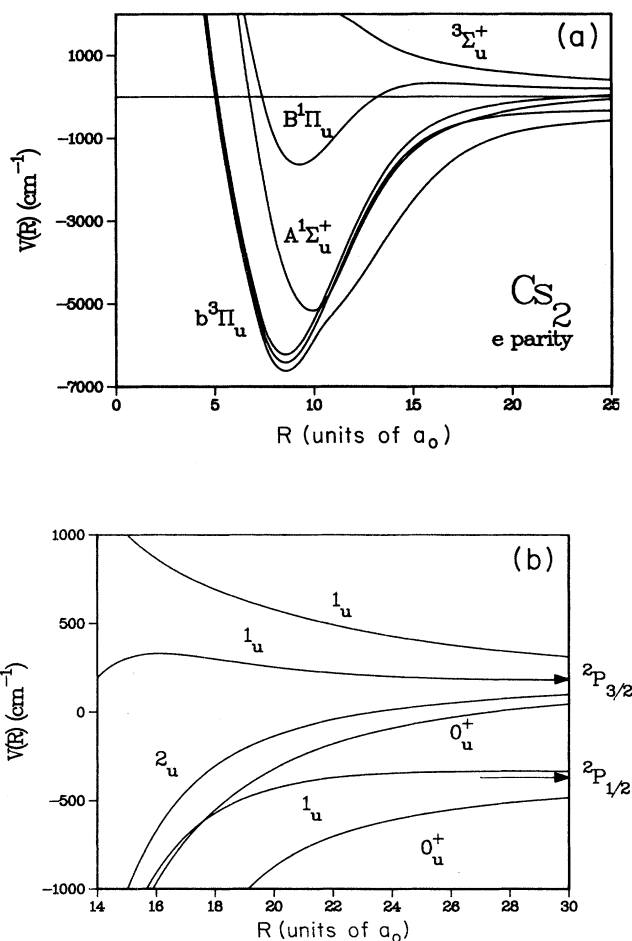


FIG. 2. (a) Fully adiabatic potential-energy curves for the  $e$ -parity states of  $\text{Cs}_2$  found by diagonalizing the electronic plus spin-orbit plus Coriolis Hamiltonian for total angular momentum  $J=2$ . Hund's case-(a) molecular symmetry labels are shown at short range. The strongly avoided crossing near  $10a_0$  is responsible for the FS transition for Cs. (b) The long-range fully adiabatic potentials, labeled by Hund's case-(c)  $\Omega$  quantum number label. The weakly avoided crossing near  $18a_0$  causes negligible FS transition probability for Cs.

TABLE II. Atomic parameters  $d^2$  in atomic units and  $\tau_0$  in  $10^{-9}$  s.

|          | Li                    | Na                    | K                     | Rb                    | Cs                    |
|----------|-----------------------|-----------------------|-----------------------|-----------------------|-----------------------|
| $d^2$    | 5.51 <sup>a</sup>     | 6.48 <sup>a</sup>     | 9.34 <sup>a</sup>     | 10.1 <sup>a</sup>     | 12.2 <sup>a</sup>     |
| $\tau_A$ | 26.9±0.8 <sup>b</sup> | 16.1±0.3 <sup>c</sup> | 27.8±0.5 <sup>c</sup> | 27.0±0.5 <sup>c</sup> | 30.5±0.7 <sup>c</sup> |
|          |                       | 16.0±0.5 <sup>d</sup> | 26.0±0.5 <sup>f</sup> | 26.0±0.5 <sup>d</sup> | 32.7±1.5 <sup>d</sup> |
|          |                       | 16.1 <sup>e</sup>     | 26.0±0.5 <sup>g</sup> | 25.8±0.8 <sup>h</sup> | 29.7±0.2 <sup>i</sup> |
|          |                       |                       | 27.3 <sup>e</sup>     | 25.7 <sup>e</sup>     | 29.4 <sup>e</sup>     |
| Present  | 27                    | 16                    | 27                    | 26                    | 30                    |

<sup>a</sup>Reference [50].<sup>b</sup>Reference [54].<sup>c</sup>Reference [55].<sup>d</sup>Reference [56].<sup>e</sup>Reference [57].<sup>f</sup>Reference [58].<sup>g</sup>Reference [59].<sup>h</sup>Reference [60].<sup>i</sup>Reference [61].

[36–38,40]. For our present purposes, we will ignore retardation effects on the potentials but will examine the effects on the molecular lifetimes. As long as  $R < R_v$  but  $R$  is large enough that  $C_3(\beta)/R^3 \ll \Delta E_{FS}$ , the  $C_3(\beta)$  coefficients and molecular lifetimes are  $R$ -independent constants. When the Hamiltonian for the electronic plus spin-orbit energy is diagonalized in this  $R$  range using well-known methods for alkali-metal dimers [48–50], the  $C_3(\beta)$  coefficients in Table I are found for each of these adiabatic entrance channels. Table II shows for each alkali-metal dimer the magnitudes of the  $d^2$  matrix elements in Table I used to calculate these long-range  $C_3(\beta)$  coefficients.

### B. Molecular spontaneous decay rates

The retardation effects on the lifetimes have been calculated in the nonrelativistic basis (neglecting electron spin) [37,38]. We have transformed these results into the asymptotically diagonalized basis of the electronic plus spin-orbit Hamiltonian. Following Meath [40], the retarded decay rate of molecular state  $\beta$  can be written as a power series:

$$A_\beta(R) = \tau_A^{-1} a(R) = \tau_A^{-1} (a_{0,\beta} + a_{2,\beta} u^2 + a_{4,\beta} u^4 \dots), \quad (39)$$

where  $u = R/R_v$  is a reduced distance parameter. An important distance is  $R_{FS} = (d^2/\Delta E_{FS})^{1/3}$ , where the interatomic interaction becomes comparable in magnitude to the asymptotic spin-orbit splitting. If  $R \gg R_{FS}$ , the  $a_{i,\beta}$  coefficients in (39) are constants independent of  $R$ , and the function  $A_\beta \tau_A$  is a universal function common to all alkali-metal pairs. Figure 3 shows this function and Table I shows the long-range coefficients in (39). Table II shows the experimental atomic lifetimes and our choice of lifetimes to be used in Sec. IV below to calculate the survival factors  $S(R, E, l, \beta)$ . Since  $R_{FS}$  ranges from  $17a_0$  for Cs to  $150a_0$  for Li, corresponding to  $u = 0.007$  and  $0.08$ , respectively, Eq. (39) with the coefficients in Table I can be used to calculate survival factors for long-range excitation near  $u = 1$ .

The series (39) through  $u^4$  terms agrees with the exact long-range formula to 0.1% or better when  $u \leq 1$ , and is only in error by about 2% when  $u = 2$ . The lead term in the expansion,  $a_{0,\beta} \tau_A^{-1} = \tau_{0,\beta}^{-1}$  in Table I, agrees with the nonretarded formulas in Table III of Movre and Pichler [62]. The decay rates of the  $0_u^+$ ,  $1_g$ , and  $0_g^-$  states are faster than the atomic decay rate, whereas the  $1_u$  state decays with a rate slower than the atom. Although spontaneous radiative decay of the  $2_u$  state is forbidden in the dipole approximation. Table II shows that at  $u = 1$  the rate is only about five times slower than for the atom. The  $2_u$  state will play an important role in the FS process for Na, K, and Rb pairs at low  $T$ .

The  $0_u^+$  and  $1_g$  states correlate at short range with the respective  $^3\Pi_u$  and  $^1\Pi_g$  chemically bound states; the  $2_u$  state also correlates with  $^3\Pi_u$ . However, the  $1_u$  and  $0_g^-$

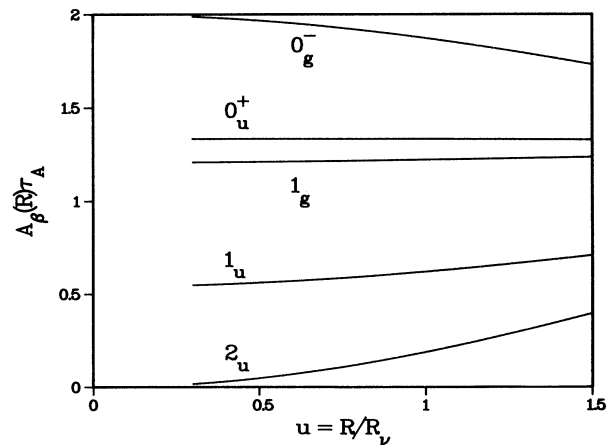


FIG. 3. Molecular decay rates, in units of the atomic decay rate  $1/\tau_A$ , vs reduced distance unit  $u$ . The  $R$  dependence is due to retardation corrections to the radiative transition probability. At small  $u$ , additional dependence on  $R$  is caused by the switching from the asymptotic Hund's case-(c) basis to the short-range Hund's case-(a) basis.

states are “pure long-range” molecular states [63] which have very shallow wells at large  $R$  before becoming repulsive at smaller distances. The  $1_u$  state adiabatically connects with the spectroscopically known  $B^1\Pi_u$  state at small  $R$ , whereas the  $0_g^-$  state becomes a component of the  $^3\Pi_g$  state. The shallowest state of the five attractive states is the  $1_u$  state, which has a minimum of 230 mK at  $R=99a_0$  for  $\text{Na}_2$  and a minimum of only 4.5 mK for Li. The deepest of the five is the  $0_g^-$  state, which has a minimum of 109 K at  $26a_0$  for  $\text{Cs}_2$ . The bound vibrational-rotational levels in the long-range wells of the  $1_u$  and  $0_g^-$  states have been calculated for the homonuclear alkali-metal dimers, except Li [63,64].

### C. Mechanisms for FS transitions

Experimental studies of the FS cross sections were carried out over 20 years ago by Krause and co-workers [65–70]. Theoretical interpretations of the possible mechanisms have also been proposed [48,71,72]. The semiclassical estimates of theoretical cross sections in all cases were found to be smaller than measured ones by a factor of 2 or more. Krause also notes that previously measured values by others are not in good agreement with his values [70]. We have recently carried out close-coupling calculations of the theoretical cross sections, and come essentially to the same conclusions as Dashevskaya [71] concerning the mechanisms and magnitudes of the cross sections. We confirm the discrepancy with the measured rate coefficients, although agreement in the case of Cs is possible when we use an approximate spin-orbit matrix element in the literature. The details of these calculations will be published elsewhere, but we will use the calculated probabilities to calculate the low-temperature collisional loss rates and the temperature dependence of the FS rate coefficient.

As Dashevskaya, Voronin, and Nikitin [48] and Nikitin [72] have clearly demonstrated, there is negligible radial coupling at long range between states of the same  $\Omega$  in the homonuclear alkali-metal dimers at room temperature. This is because the slowly varying long-range  $1/R^3$  potential leads to an adiabaticity parameter much larger than 1, and there is no possibility of transitions between states of the same  $\Omega$ . This is in strong contrast to the case of alkali-metal–rare-gas collisions, where radial derivative coupling between states of the same symmetry leads to large transition probabilities [72]. One demonstration of this is seen in the photodissociation of the  $B^1\Pi_u$  state of alkali-metal dimers. The relative yields of the  $^2P_{3/2}$  and  $^2P_{1/2}$  products have been measured in several experiments [73–81]. In some cases, the only detected product is  $^2P_{3/2}$ , with a  $^2P_{1/2}$  yield smaller than 1% [73,76–78,80,81]. Gerber and Moller [80] have explained observations of comparable products in both channels as a consequence of two-photon excitation of upper electronic states. Theoretical calculations of photodissociation branching ratios for  $\text{K}_2$  [81,82] have also demonstrated that the branching is almost entirely to the  $^2P_{3/2}$  channel, with which the  $B^1\Pi_u$  state correlates adiabatically. Conversely, photodissociation through the  $A^1\Sigma_u^+$  state of  $\text{Na}_2$  has been calculated [83] to yield al-

most entirely  $^2P_{1/2}$  product atoms with which the  $A$  state correlates adiabatically.

The gerade electronic states contribute an insignificant fraction of the cross section. The only significant  $g$ -state mechanism is the crossing of the  $1_g$  state from  $^2P_{3/2}$  and the  $0_g^+$  state from  $^2P_{1/2}$ . Dashevskaya, Voronin, and Nikitin [48] have shown the matrix element and transition probability to be small from this long-range crossing. Our close-coupling calculations show the contribution to  $\sigma$  at room temperature from all the  $g$  states to be less than  $1a_0^2$  for K, Rb, and Cs, and only about  $10a_0^2$  for the light molecule Na. There is a possible small contribution at elevated temperature due to the short-range crossing of the  $^1\Sigma_g^+$  and  $^3\Pi_g$  curves seen in *ab initio* calculations [47]. However, the  $^1\Sigma_g^+$  potential has a barrier which prevents FS transitions except at elevated temperatures. We estimate that even this mechanism is insignificant except possibly for K at elevated temperatures.

Therefore, only the  $0_u^+$  and  $2_u$  states from  $^2P_{3/2}$  are entrance channel states which give appreciable contributions to the FS cross section [see Fig. 2(b)]. There are three basic mechanisms, described by Dashevskaya [71], which can contribute: (1) spin-orbit mixing of the  $0_u^+$  components of the  $A^1\Sigma_u^+$  and  $b^3\Pi_u$  states at their crossing near the minimum of the  $A^1\Sigma_u^+$  potential [see Figs. 1(a) and 2(a)], (2) Coriolis mixing of the components of the  $b^3\Pi$  state at short range, (3) Coriolis mixing of the  $0_u^+$  and  $1_u$  states at their long-range crossing. Only the  $0_u^+$  entrance channel state contributes to all three mechanisms; the  $2_u$  entrance channel state also contributes to mechanism 2. The alkali-metal species divide into two distinct classes. The dominant mechanisms at room temperature for the light species Na and K with relatively small spin-orbit matrix elements are the Coriolis mechanisms (2) and (3), whereas the spin-orbit mechanism (1) gives only a small contribution. The opposite applies to the heavy species Rb and Cs with large spin-orbit matrix elements, that is, only mechanism (1) is dominant at room temperature. Since mechanisms 1 and 2 only occur in the inner chemical zone of interaction where the atoms are close together, we expect the rate coefficient to be a product of the Langevin capture rate coefficient times the average channel FS probability, as in Eq. (17). We will illustrate this theory for the case of Cs FS transitions by mechanism 1 using the ECP potentials of Krauss and Stevens [47]. We set up the  $2 \times 2$  Hamiltonian matrix for the  $0_u^+$  states in terms of the nonrelativistic  $^1\Sigma_u^+$  and  $^1\Pi_u$  potentials and the asymptotic spin-orbit splitting [48–50]. The FS probability is determined by the Hund’s case (a) spin-orbit matrix element,  $V_{\text{SO}} = \langle A^1\Sigma_u^+(0_u^+) | H_{\text{SO}} | b^3\Pi_u(0_u^+) \rangle$  at the crossing of the two nonrelativistic potentials near  $10a_0$  (see Fig. 1). If this spin-orbit matrix element does not vary with  $R$ , its magnitude is related to the asymptotic fine-structure splitting by [84]

$$V_{\text{SO}} = 2^{1/2} \Delta E_{\text{FS}} / 3 = 0.471 \Delta E_{\text{FS}} . \quad (40)$$

However, deperturbation analysis of high-resolution spectroscopic data for  $\text{Li}_2$ ,  $\text{Na}_2$ , and  $\text{K}_2$  found  $V_{\text{SO}}$  to be,

respectively, 0.338, 0.343, and 0.318 times  $\Delta E_{\text{FS}}$  [84–86]. These values are only 70% of the value predicted by (40). The near constancy of the measured scaling factor for  $\text{Li}_2$ ,  $\text{Na}_2$ , and  $\text{K}_2$  suggests that the same scaling may be applied to  $\text{Rb}_2$  and  $\text{Cs}_2$ . Assuming a scaling factor of 0.34 instead of 0.471 gives estimated  $V_{\text{SO}}$  values of 81 and  $188 \text{ cm}^{-1}$  for  $\text{Rb}_2$  and  $\text{Cs}_2$ , respectively. O’Callahan, Gallagher, and Holstein [87] estimated a value of  $150 \text{ cm}^{-1}$  for  $\text{Cs}_2$  based on fitting the low-resolution absorption spectrum of  $\text{Cs}_2$  with a nonadiabatic strong coupling model which accounts for the avoided crossing of the  $0_u^+$  components of the  $A$  and  $b$  potentials [Fig. 2(a)]. This magnitude corresponds to a scaling factor of 0.27 instead of 0.34.

We have carried out a standard quantum-mechanical two-channel close-coupling calculation of the cross section for the  ${}^2P_{3/2} \rightarrow {}^2P_{1/2}$  FS process for Cs collisions. The spherically averaged cross section to be compared to cell experiments is  $\frac{1}{16}$  of the  $0_u^+$  channel cross section defined by Eq. (10) [see comment after Eq. (14)]. The mean FS probability  $\bar{P}$  for the  $0_u^+$  channel is defined by Eq. (19). Calculations were done using both spin-orbit matrix elements, 188 and  $150 \text{ cm}^{-1}$ . Figure 4 shows the quantum opacity function  $P(E, l, 0_u^+)$  as a function of  $l$  at a collision energy of  $E/k_B = 300 \text{ K}$  when  $V_{\text{SO}}$  is chosen to be  $150 \text{ cm}^{-1}$ . The sharp cutoff at  $l_{\text{max}}$  is evident in the figure. The primary effect of lowering  $E$  is to lower the value of  $l_{\text{max}}$  as  $E$  decreases. Equations (15) and (16) show that  $l_{\text{max}}$  varies quite slowly with  $E$ , as  $E^{1/6}$ . The mean probability  $P(E)$  is nearly independent of  $E$ , only varying from 0.41 to 0.43 as  $E/k_B$  decreases from 300 K to 1 mK, an energy range of nearly six orders of magnitude. These observations demonstrate that Eq. (17) using the Langevin capture rate is an excellent approximation for Cs FS collisions. When we take  $V_{\text{SO}} = 188 \text{ cm}^{-1}$ ,

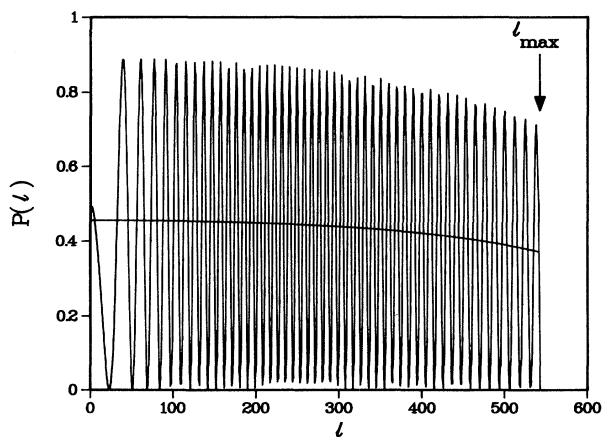


FIG. 4. Calculated quantum (oscillating) and semiclassical (line) probability of FS transitions for the spin-orbit induced FS transition in Cs, calculated at  $E/k_B = 300 \text{ K}$ . The sharp cutoff at  $l_{\text{max}} = 540$  due to the barrier in the  $0_u^+$  entrance channel potential is evident in the calculation.

$\overline{P(E)}$  varies from 0.24 to 0.29 over the same range of energy. Note that  $\bar{P}$  is actually larger when the smaller  $V_{\text{SO}}$  is used. When a full six-channel close-coupling calculation is done which includes all four *ungerade* potentials and the effects of Coriolis coupling, these probabilities are only increased by 5% or less. Therefore, Coriolis coupling is insignificant for Cs FS collisions, and the simpler two-channel model is sufficient to calculate the FS rate coefficient.

The above results are readily understood by using the familiar Landau-Zener curve crossing formula,

$$P = 2e^{-A}(1 - e^{-A}), \quad (41)$$

where

$$A = 2\pi V^{*2} / (\hbar v^* D^*) \quad (42)$$

and  $V^*$ ,  $v^*$ , and  $D^*$  are the respective coupling matrix element, velocity, and slope difference of the potential curves at the crossing point  $R^*$  of the two curves. The semiclassical probability shown in Fig. 4 is in excellent agreement with the quantum probability averaged over oscillations. The maximum probability in Eq. (41) occurs when  $A = \ln 2 = 0.693$ . Since  $A > 0.693$  for  $\text{Cs}_2$ , the passage through the crossing tends to be adiabatic on the diagonalized potentials, and the probability is actually *larger* with the *smaller* spin-orbit matrix element, as found in the quantal calculation. This is because the smaller matrix element reduces the adiabaticity parameter  $A$  and leads to a larger  $P$  in (41).

The calculated cell cross section for Cs FS collisions at 300 K are  $120a_0^2$  and  $68a_0^2$  when the respective 150 and  $188\text{-cm}^{-1}$   $V_{\text{SO}}$  are used. Since the measured cross section is  $110a_0^2$ , better agreement is obtained when the  $150\text{-cm}^{-1}$  matrix element estimated by O’Callahan, Gallagher, and Holstein [87] is used. However, the magnitude of the experimental error is uncertain, and Cs is the only alkali-metal species for which such good agreement can be obtained between our close-coupled calculations and experiment (see below). Therefore, some question remains whether the agreement between theory and experiment for Cs may be partly fortuitous. It is clearly desirable to obtain  $V_{\text{SO}}$  by more reliable means, either by high-resolution spectroscopic analysis or from careful *ab initio* treatment.

We have also carried out two- and six-channel close-coupled calculations for  $\text{Rb}_2$ , using the scaled  $V_{\text{SO}} = 81 \text{ cm}^{-1}$ , and six-channel calculation for  $\text{Na}_2$  and  $\text{K}_2$ , using the measured  $V_{\text{SO}}$ . The calculated cell average cross section at  $E/k_B = 300 \text{ K}$  for Rb FS collisions is  $95a_0^2$  for the two-channel calculation. The cross section is increased by 40% in the six-channel calculation which includes Coriolis coupling. The increase is due to partial waves with large  $l$ , near  $l_{\text{max}}$ , since the probability due to Coriolis coupling increases approximately as  $l^2$ . Our six-channel cross section is about 25% larger than the rough semiclassical estimate of Dashevskaya [71], and is about a factor of 2 smaller than the measured value of  $240a_0^2$ .

In contrast to  $\text{Cs}_2$  and  $\text{Rb}_2$ , the dominant mechanism of the fine-structure-changing transition in  $\text{Na}_2$  and  $\text{K}_2$  at normal temperatures is Coriolis coupling. The spin-orbit

TABLE III. Calculated FS probabilities at  $E/k_B=1$  mK.

| Species | $\beta=0_u^+$               |            |                         | $\beta=2_u$                 |            |                         |
|---------|-----------------------------|------------|-------------------------|-----------------------------|------------|-------------------------|
|         | $P(E,l,\beta)$              | $l_{\max}$ | $\overline{P(E,\beta)}$ | $P(E,l,\beta)$              | $l_{\max}$ | $\overline{P(E,\beta)}$ |
| Na      | $2.5 \times 10^{-4} l(l+1)$ | 23         | 0.066                   | $3.2 \times 10^{-4} l(l+1)$ | 19         | 0.064                   |
| K       | $1.9 \times 10^{-4} l(l+1)$ | 34         | 0.12                    | $1.1 \times 10^{-4} l(l+1)$ | 29         | 0.049                   |
| Rb      | 0.36                        | 52         | 0.36                    | $7.5 \times 10^{-6} l(l+1)$ | 45         | 0.0079                  |
| Cs      | 0.28                        | 70         | 0.28                    | $9 \times 10^{-9} l(l+1)$   | 59         | $10^{-5}$               |

mechanism, which is so important for  $\text{Rb}_2$  and  $\text{Cs}_2$ , contributes only a small fraction of the cross section in these lighter alkali-metal species. At long range the  $0_u^+$  state from  ${}^2P_{3/2}$  is crossed by the  $1_u$  state which correlates with  ${}^2P_{1/2}$ . At short range both the  $0_u^+$  and  $2_u$  states from  ${}^2P_{3/2}$  become components of the  ${}^3\Pi_u$  state, and mix with the  $1_u$  component of this state which connects with  ${}^2P_{1/2}$  asymptotically. This short-range mixing is that which is responsible for the transition from Hund's case (a) to Hund's case (b) in the  ${}^3\Pi_u$  state. We have verified the dominance of the Coriolis mechanisms by full close-coupled calculations with model potentials for  $\text{Na}_2$  and  $\text{K}_2$  which include the contributions of all three mechanisms. We find cross sections of similar magnitude to those of Dashevskaya [71], which are also about a factor of 2 smaller than the measured ones for these alkali-metal species. We find large mean probabilities, on the order of 0.5–1, for a large range of partial waves below the cutoff value  $l_{\max}$ . However, the probability drops off rapidly as  $l \rightarrow 0$  because the Coriolis coupling operator is approximately proportional to  $l$ .

Table III summarizes for all four alkali-metal species the results of the close-coupled calculation of  $P(E,l,\beta)$  at low collision energy for the  $0_u^+$  and  $2_u$  entrance channels (probability per nondegenerate component in the case of

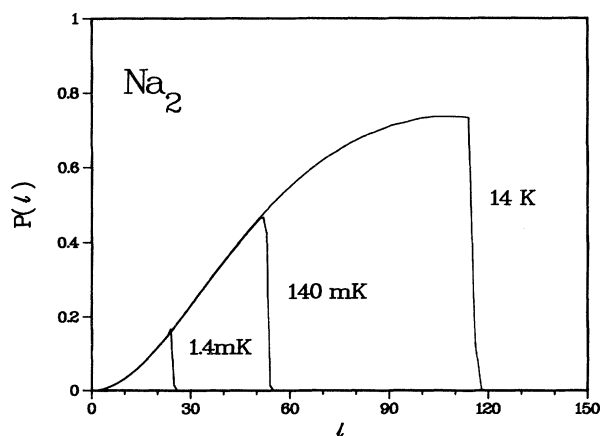


FIG. 5. Calculated quantum probability of the FS transition for the  $2_u$  channel of  $f$  molecular parity for three different collision energies  $E/k_B$  for Na collisions. The rapid increase with angular momentum  $l$  is a consequence of the Coriolis mechanism. The sharp cutoff at  $l_{\max}$  is evident at each energy. Below the cutoff, the probability is insensitive to energy.

$2_u$ ). Figure 5 illustrates the feature that the probability of the Coriolis mechanism at fixed  $l$  is nearly independent of  $E$  at low collision energy, as long as  $l$  remains less than  $l_{\max}$ . The probability for the Coriolis mechanisms can be approximately represented as  $P(E,l,\beta) = p_0(\beta)l(l+1)$ , where  $p_0$  is independent of the collision energy  $E$  and is found by fitting the calculated probabilities. Table III also gives  $l_{\max}$  and the mean probability, Eq. (19), at  $E/k_B=1$  mK. Note that  $l_{\max} \gg 1$  in all cases, implying that this low  $T$  is still very large compared to the temperature where only  $s$  waves ( $l=0$ ) contribute in the quantum threshold limit [23]. The calculated  $\overline{P}$  for Na, averaged over the eight attractive entrance channels, is  $[0.066 + (2)0.064]/8 = 0.024$ , which is over an order of magnitude smaller than the value assumed by GP for their single “effective” attractive state [21]. This is because extrapolation from room temperature to ultracold temperature is invalid for the case of Coriolis coupling. This is one of the features missed by the original GP theory. It is significant because we show below that the Coriolis mechanism is the dominant one for FS at low  $T$  for all alkali-metal species except Cs.

#### D. Rate coefficients for RE transitions

The spectrum of emitted light for the RE process, Eq. (1), as a function of the red shift  $\Delta E$  in Eq. (3) is calculated from Eqs. (10) and (14) from the spectral probability density due to entrance channel  $\beta$  [88,89]:

$$P_S(E,l,\beta \rightarrow f; \Delta E) \quad (43a)$$

$$= h(64\pi^4/3h\lambda^3) |\langle E,l,\beta | d(R) | E_f,l,f \rangle|^2$$

$$= h A_\beta |\langle E,l,\beta | E_f,l,f \rangle|^2, \quad (43b)$$

where  $d(R)$  is the transition dipole moment, and the second expression (43b) in terms of the Einstein coefficient  $A_\beta$  applies if  $d(R)$  is independent of  $R$ . Here the index  $f$  implies summing over all ground-state molecular components. The probability of emitting a photon with shift between  $\Delta E$  and  $\Delta E + d(\Delta E)$  is  $P_S d(\Delta E)$ , and  $P_S$  has units of energy $^{-1}$ . The probability of emitting a photon which leads to RE is obtained by integrating the spectral probability  $P_S$  over all  $\Delta E$  greater than some minimum  $\Delta_{\text{RE}}$  which defines the escape energy in Eq. (3):

$$P(E,l,\beta \rightarrow f; \Delta_{\text{RE}}) = \int_{\Delta_{\text{RE}}}^{\infty} P_S(E,l,\beta \rightarrow f; \Delta E) d(\Delta E). \quad (44)$$

An extremely useful approach to the RE process is to introduce the semiclassical approximations which lead to the quasistatic picture [89–91]. The classical Franck-Condon principle is satisfied at the stationary phase point  $R^*$  at which the emitted photon energy matches the difference potential. Since the ground state is flat at large  $R$ , the red shift is just the excited-state attraction:

$$\Delta E = C(\beta)/R^{*3}. \quad (45)$$

By introducing the usual stationary-phase and random-phase approximations for the integral in (42), the semiclassical approximation is readily derived (assuming only a single  $R^*$  point) [91]:

$$|\langle E, l, \beta | d(R) | E_f, l, f \rangle|^2 \approx \frac{2d(R^*)^2}{hv^*(E, l)D^*(\beta, f)}, \quad (46)$$

where  $v^*$  and  $D^*$  are the respective velocity and potential slope difference at  $R^*$ . Upon noting that  $d(\Delta E) = D^*dR$ , Eqs. (43) and (46) immediately lead to an expression with a simple and obvious physical interpretation:

$$P(E, l, \beta \rightarrow f; \Delta_{\text{RE}}) = \int_{-t^*}^{t^*} A_{\beta f}(t) dt. \quad (47)$$

Equation (47) gives the probability of spontaneously emitting a photon with  $\Delta E > \Delta_{\text{RE}}$  over the classical trajectory from  $R^*$  to the inner turning point and back to  $R^*$ . The probability (47) will be much less than unity as long as the passage time  $2t^*$  is short compared to the decay lifetime  $A_{\beta}^{-1}$ .

An escape energy  $\Delta_{\text{RE}}$  permits escape from a trap  $\Delta_{\text{RE}}/2k_B$  deep, since both atoms share the kinetic energy equally. We will assume  $\Delta_{\text{RE}}/2k_B$  has the order of magnitude 1 K. Since  $\Delta_{\text{RE}} \gg E$  and  $\delta$  in the low-temperature limit, the excitation occurs at a very long range beyond the centrifugal barrier position  $R_C(\beta)$ , whereas  $R^*$  will lie well inside  $R_C(\beta)$ . Thus, the channel spectral rate coefficient for photon emission, uncorrected for spontaneous emission losses, is

$$K_S(E, \beta \rightarrow f; \Delta E) = K_C(E, \beta) \overline{P_S(E, \beta \rightarrow f; \Delta E)}, \quad (48)$$

where  $\overline{P_S}$  is averaged over  $l$ , Eq. (19). For all alkali-metal pairs except Li (see below) almost the whole spectrum comes within the interval  $R_{\text{FS}} \ll R^* \ll R_C(\beta)$ , and  $A_{\beta}$  is given by the parameters in Table I. Using Eqs. (45) and (46), the semiclassical approximation to the spectral probability

$$\begin{aligned} \overline{P_S(\beta \rightarrow f; \Delta E)} \\ = (2^{1/2}/3) A_{\beta} \mu^{1/2} C_3(\beta)^{1/3} / \Delta E^{11/6} \quad (E \ll \Delta E) \end{aligned} \quad (49)$$

is independent of the incident energy in this low-temperature limit. We have verified by direct numerical calculation [19,26] that the spectrum calculated from (49) passes through the center of the quantum oscillations of the spectrum calculated from the quantum probabilities (43).

The spectrally integrated probability from Eq. (44) for

emission with  $\Delta E \geq \Delta_{\text{RE}}$  is

$$\overline{P(\beta \rightarrow f; \Delta_{\text{RE}})} = (2^{3/2}/5) A_{\beta} \mu^{1/2} C_3(\beta)^{1/3} / \Delta_{\text{RE}}^{5/6}, \quad (50)$$

and the corresponding channel rate coefficient for calculating the photon production rate per unit volume is

$$\begin{aligned} K(E, \beta \rightarrow f; \Delta_{\text{RE}}) &= K_C(E, \beta) \overline{P(\beta \rightarrow f; \Delta_{\text{RE}})} \\ &= \frac{6\pi 2^{1/2}}{5} \frac{A_{\beta} C_3(\beta)}{\Delta_{\text{RE}}^{5/6} (2E)^{1/6}}. \end{aligned} \quad (51)$$

The thermal average is found by making the replacement in Eq. (20). After Eq. (51) is used in Eq. (28) to do a low-temperature spherical average for cell conditions, the rate coefficient gives the emission rate of photons with a red shift larger than  $\Delta_{\text{RE}}$ , or equivalently, the loss rate of excited  $P$  atoms. The RE contribution to the trap-loss rate should be twice this, since two hot atoms appear per photon emitted.

Since the  $2_u$  state makes negligible contributions to RE for all alkali-metal species because of the very small decay rate in the region of  $R^*$  where the RE emission occurs, the  $A_{\beta}$  factor in the spectral probability  $\overline{P_S}$  or  $\overline{P}$  in Eqs. (49) or (50) is just the  $a_{0,\beta}$  factor in Eq. (39). Except for Li,  $a_{0,\beta}$  can be taken as an  $R$ -independent constant. Since  $R^* \ll R_{\text{FS}}$  for Li due to the extremely small  $\Delta E_{\text{FS}} = 0.3353 \text{ cm}^{-1}$  [92], the actual  $R$ -dependent short-range Hund's case-(a) form of the potentials and  $a_{0,\beta}$  coefficients must be used for Li. Only two states are chemically bound enough to give a 1-K red shift for RE in Li, namely, the  $0_u^+$  and  $1_g$  states. The former correlates at short range with  $^3\Pi_u$  and the latter with  $^1\Pi_g$ . Both have potentials that vary as  $d^2/R^3$  when  $R \ll R_{\text{FS}}$ . Although the decay rates vanish in a pure Hund's case-(a) basis, both of these states have small decay rates that can readily be worked out using perturbation theory when  $R < R_{\text{FS}}$ . Defining

$$X = \frac{d^2}{3\Delta E_{\text{FS}} R^3} \quad (52)$$

and neglecting small terms in  $u^2$ , we find in the  $R$  range of interest for the  $\text{Li}_2$  molecule,

$$A(1_g) = \tau_A^{-1} \frac{5}{162X^2} \quad (X \geq 1) \quad (53)$$

$$A(0_u^+) = \tau_A^{-1} \frac{4}{(9X-1)^2} \quad (X \geq 1). \quad (54)$$

These should be used in Eqs. (49) instead of a constant  $a_{0,\beta}$ . Since  $\Delta E = d^2/R^3$ , we see from Eqs. (52)–(54) that  $A$  varies inversely as  $(\Delta E)^2$ . This fact allows us to integrate (49) to get a new Eq. (50) for the probability. The probability for Li is just  $\frac{5}{17}$  times  $\overline{P}$  in Eq. (50) with  $C(\beta) = d^2$  and Eqs. (53) and (54) above used for  $A_{\beta}$ . Note that the RE rate coefficient scales as  $\Delta_{\text{RE}}^{-17/6}$  for Li, whereas it scales as  $\Delta_{\text{RE}}^{-5/6}$  for all the other alkali-metal species.

#### IV. CALCULATION OF RATE COEFFICIENTS

##### A. Problems in low-temperature calculations

Given the long-range potential and lifetime parameters in Tables I and II, the FS probabilities in Table III, and the RE probabilities from Eqs. (50), (53), and (54), it is a straightforward matter to evaluate numerically  $K_C$ ,  $\bar{P}$ , and the excitation and survival integral  $I$  for each entrance channel and calculate the rate coefficients  $K^*$  and  $K_g$  in Eqs. (26)–(28). However, in order to calculate  $I(E)$  at low temperature there are two problems that need to be resolved. The first is simple to fix. If  $E$  is low enough that the ground-state cutoff applies to the numerator in Eq. (32), there will always be singularities in the denominator at discrete  $R$  values for each  $l$  where  $v(E, R, l)$  vanishes at the classical turning point. This occurs when  $E/k_B$  is on the order of 1 mK or less. One way to avoid this problem is to convert  $l$  to a continuous variable and use Eq. (A7) in Appendix A to integrate the integrable singularity. The other way, which we use here, is to keep the discrete sum, but not to allow  $v/v(E, R, l)$  to be larger than some maximum value near a singularity. Our choice of maximum value of 4 for this ratio leads to insignificant errors in the integral  $I(E)$ .

The second problem is more fundamental. It has to do with the choice of initial kinetic energy  $E'(R)$  for motion on the upper potential. This choice is critical for calculating the survival probability, Eq. (25). In the usual scattering picture with a conservative Hamiltonian and no spontaneous emission the molecular transition is from an initial state with asymptotic kinetic energy  $E$  to a final state with asymptotic kinetic energy  $E'$ , and the transition amplitude is proportional to the Born distorted wave matrix element  $\langle \Psi^-(E') | \hat{\epsilon}_0 \cdot \mathbf{d} | \Psi^+(E) \rangle$ . Since the broadening due to the finite lifetime of the excited state is neglected, energy conservation for the overall collision requires that  $E' = E - \delta$ . This is the normal scattering picture for a collision in a weak radiation field [93,94]. In this picture the classical Franck-Condon principle, requiring no change in local kinetic energy at the distance  $R$  where the transition “occurs,” is satisfied only at the Condon point  $R_C$ , where the difference between upper and lower potentials matches the detuning  $\delta$  of the excitation laser. But the excitation function  $\epsilon(R, \beta)$  in Eq. (23), which accounts for the finite lifetime broadening of the excited state, allows local *off-resonant* excitation for which the semiclassical trajectory must violate *either* the above conventional energy conservation requirement *or* the local classical Franck-Condon principle. The dilemma posed by the semiclassical framework adopted by GP and us simply reflects the necessity, discussed in Sec. II B of the formulation of a proper collision theory which includes the broadening due to radiative decay. The problem only occurs in ultracold collisions because  $E$ ,  $\delta$ , and  $h\gamma_A$  are all of comparable size. Therefore, we have tried calculations using two possible choices of initial kinetic energy  $E'(R)$  for excitation at  $R$ : the first satisfies the overall energy-conservation requirement of scattering theory but violates the classical Franck-Condon principle, except at  $R$ :

$$E'(R) = E - \frac{\hbar^2 l(l+1)}{2\mu R^2} + \left[ \frac{C(\beta)}{R^3} - \delta \right], \quad (55)$$

whereas the second satisfies “local” energy conservation and the classical Franck-Condon principle at  $R$ :

$$E'(R) = E - \frac{\hbar^2 l(l+1)}{2\mu R^2}. \quad (56)$$

In either case,  $E'(R)$  serves as the initial kinetic energy for calculating the time integral in the survival factor  $S(R, E, l, \beta)$ . The two choices are equivalent only when  $R = R_C$ , where  $\delta = C(\beta)/R^3$ . The second choice seems more consistent with the spirit of the semiclassical theory, but it is not obvious which makes the better *a priori* choice. The calculations below for the various alkali-metal species will examine the consequences of both choices.

##### B. Trap-loss and FS rate coefficients for Cs

The only alkali-metal species for which the trap-loss rate coefficient has been unambiguously measured is Cs [22]. The measurements were carefully carried out under low-density conditions that excluded density nonuniformities associated with collective effects [95]. The trap temperature was in the range 250–400  $\mu$ K. Once the laser power was high enough to exclude loss processes that were presumably due to collisional changes in ground-state hyperfine level, the experimental loss rate was found to be linear in laser power, in agreement with the weak-field excitation assumption of our theory and that of GP. A rate coefficient calculated for the GP theory was reported which was about a factor of 4 smaller than the measured value. We will examine the Cs case in some detail to illustrate the basic feature of the temperature dependence of the rate coefficient.

Figure 6 illustrates the excitation and survival com-

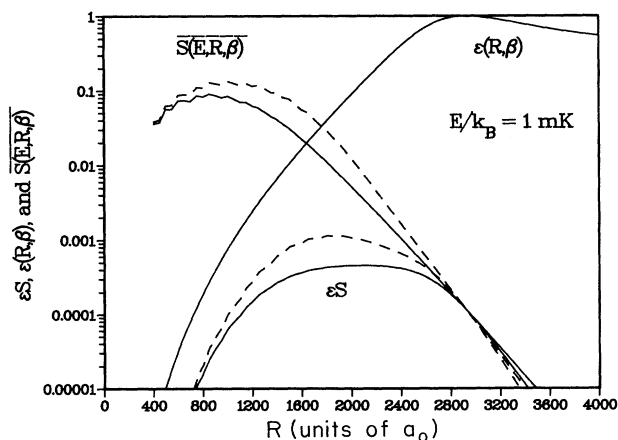


FIG. 6. Absorption and survival factors in the integrand of the  $I(E, \beta)$  function for the  $0_u^+$  entrance channel for  $\text{Cs}_2$  for a detuning of one linewidth. The solid and dashed lines for the average survival factor correspond to respective choices of Eqs. (56) and (55) for the initial kinetic energy to calculate the survival factor.

ponents of the integrand in the excitation/survival factor  $I(E, 0_u^+)$  of Eq. (30). The absorption factor  $\epsilon(R, 0_u^+)$  peaks at unity at the Condon point  $R_C$  near  $2800a_0$ . The two curves for the average survival factor  $S(R, E, 0_u^+)$  reflect the two choices in Eqs. (55) and (56). These curves agree at  $R_C$ , but the larger initial kinetic energy for the first choice results in better survival when  $R < R_C$ . The two again agree at small  $R$ , since the survival probability is high and is more determined by the strong acceleration by the attractive potential than by the initial velocity. The small "oscillations" in  $\bar{S}$  at small  $R$  are due to the fact that we evaluate the sum over  $l$  using discrete  $l$  values rather than the continuous classical representation of Eq. (A7).

Figure 7 illustrates the dependence of the individual survival factors on  $l$  for short-, intermediate-, and long-range values of  $R$ . A rapid decrease of  $S(l)$  with increasing  $l$  is evident at the larger  $R$  values. This is because the kinetic energy along the trajectory decreases with increasing  $l$ , causing an increase in propagation time to small  $R$ . Since the survival factor  $S_{GP}$  in the GP expression, Eq. (37), is independent of  $l$  and calculated for  $l=0$ ,  $S_{GP}$  always overestimates the average survival factor, given the same potential parameters. Figure 6 also shows that  $S(R, E, 0_u^+)$  reaches a maximum of only 0.1 near  $800a_0$  and then actually decreases to smaller  $R$ . Since the average survival factor is defined as the average over the 70 partial waves  $l$  that contribute to  $K_C$  for a 1-mK excited-state collision, this decrease occurs because at small  $R$  the ground-state centrifugal potential excludes the higher partial waves, thereby reducing the average.

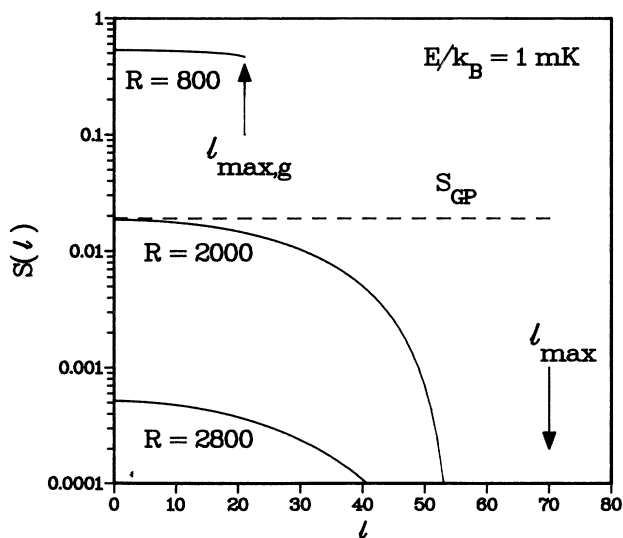


FIG. 7. Individual survival factors  $S(R, E, l, \beta)$  for  $E/k_B = 1$  mK vs  $l$  for the  $0_u^+$  entrance channel in  $\text{Cs}_2$ , calculated for three different distances  $R$  and a detuning of one linewidth. The dashed line shows the  $l$ -independent survival factor of the GP expression, calculated with the same potential and lifetime.

For example, at  $R = 400a_0$ , only 11 partial waves contribute to the numerator in Eq. (32), causing a decrease in the average  $\bar{S}$  despite the fact that the individual  $S(R, E, l, 0_u^+)$  factors are near unity for the partial waves that contribute (see Fig. 7).

Figure 8 illustrates the temperature dependence of the excitation and survival integral  $I(E, 0_u^+)$  for three different detunings  $\delta$ , using the choice in Eq. (56) to calculate the survival factors. Since evaluation at high  $T$  requires integration to large distances where  $u = R/R_v \gg 1$ , the exact retarded expression was used for the radiative decay rate rather than the short-range expansion in Table I:

$$A(R, 0_u^+) \tau_A = 1 - \frac{\sin u}{2u} - 5 \frac{\cos u}{2u^2} + 5 \frac{\sin u}{2u^3}. \quad (57)$$

For detunings larger than about  $h\gamma_A$  Fig. 8 shows that  $I(E)$  actually is larger than unity over a range of  $E$ . This is because the molecule can be excited on resonance near  $R_C$  during the collision, whereas the atom is excited off resonance. At sufficiently high temperature, the phase space near  $R_C$  makes only a small contribution to  $I$  and  $I$  approaches unity as required. At sufficiently low  $T$ , survival losses cause a decrease in  $I$  and a consequent decrease in the effective rate coefficient by several orders of magnitude.

In order to compare the predictions of our theory with that of the simpler GP formulas, Eqs. (36)–(38), it is necessary to compare entities that are equivalent except for the approximations employed. It is best to eliminate the part that depends on assumptions about FS probabilities and compare only the part which counts the contributing phase space weighted by excitation and survival. This is done in Fig. 9, which compares the directly comparable quantities  $K_C(E, 0_u^+)I(E, 0_u^+)$  and  $I_{GP}(E, 0_u^+)/2\tau_A$ . The  $K^*$  rate coefficient is found from either of these

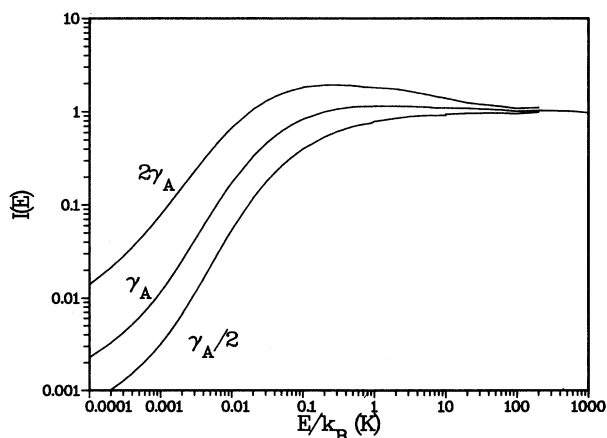


FIG. 8. Collision energy dependence of the excitation and survival correction factor  $I(E, \beta)$  for the  $0_u^+$  state of  $\text{Cs}_2$ , shown for three different values of the detuning  $\delta/h$ .

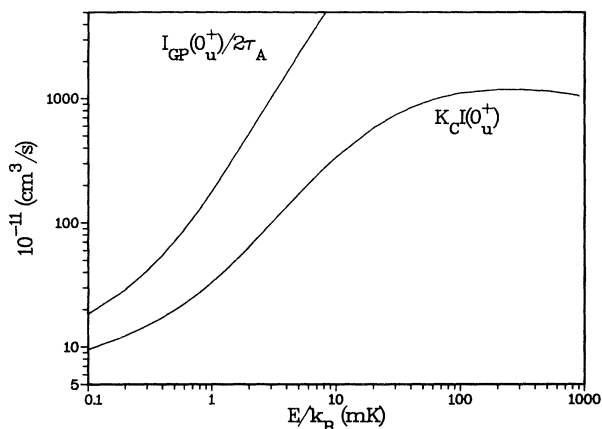


FIG. 9. Comparison of the predictions of our rate expression, Eq. (28), vs the GP expression, Eq. (36), for the  $0_u^+$  entrance channel in  $\text{Cs}_2$  and a detuning of one linewidth. These should be multiplied by a common degeneracy-averaged FS probability to convert to an actual rate coefficient.

by multiplying by the channel averaged FS probability. The two solid lines show the results when both expressions use the local Franck-Condon choice of initial kinetic energy and the same  $C(\beta)$  and  $A_\beta$  parameters. The GP formula is larger than ours below 1 mK because their survival factor is too large for the reasons given in conjunction with Figs. 6 and 7. As  $T$  increases, the GP expression rapidly becomes too large because it overcounts phase space by neglecting to cut off the  $l$  sum at the excited state  $l_{\text{max}}$ . Of course, the GP expression was never intended for use at temperatures above ultracold.

Figure 10 illustrates the temperature dependence of the cell-averaged  $K^*$  rate coefficient for the FS transition in Cs for a detuning of one linewidth. The solid curve labeled  $L$  was calculated using the choice of  $E$  which satisfies the local Franck-Condon principle, Eq. (56). The dashed line labeled  $G$  was calculated using the choice of overall energy conservation, Eq. (55). The two agree above about 10 mK, but differ at lower  $T$  for the reasons given in the discussion of Fig. 6. The upper dashed curve labeled  $C$  shows the Langevin capture rate coefficient for FS collisions,  $K_C(E, 0_u^+)P(0_u^+)/16$ . The room-temperature rate coefficient agrees with the measured value, as discussed in Sec. III C. The prominent feature of Fig. 10 is the rapid decrease of  $K^*$  below about 100 mK as excited-state survival probability becomes poorer with decreasing collision energy. The calculated trap-loss rate coefficient can be compared to the measured value using Eq. (27) to relate  $K^*$  and  $K_g$ . The loss rate  $K_{\text{loss}}$  is  $2K_g$ , where both FS and RE contributions are included in  $K_g$ . At a laser power of 10 mW/cm<sup>2</sup>,  $K_{\text{loss}} = 1.1K^*$  for Cs. Figure 10 compares the measured [22] and calculated rate coefficients for the Cs trap near 300  $\mu\text{K}$ . A value of  $\Delta_{\text{RE}}/2k_B = 1$  K was chosen for the RE energy. The RE rate scales as  $\Delta_{\text{RE}}^{-5/6}$  and at 300  $\mu\text{K}$  is calculated to con-

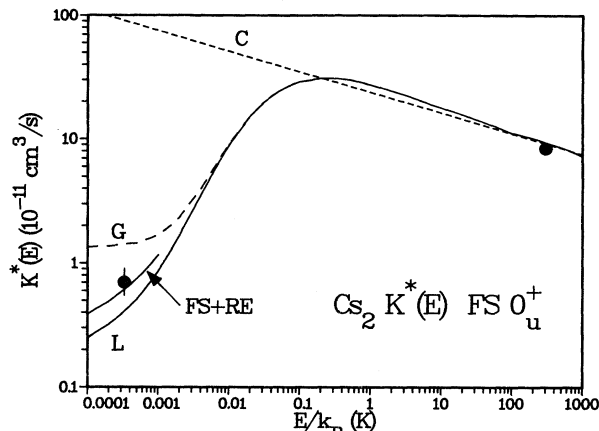


FIG. 10. Collision energy dependence of the effective excited-state cell-averaged FS rate coefficient for Cs collisions. The low-temperature curves labeled  $G$  and  $L$  correspond respectively to initial energy choices of “global” energy conservation, Eq. (55), and “local” energy conservation, Eq. (56). Experimental points are shown for 300 K and 300  $\mu\text{K}$ . The calculated rate including RE loss is also shown at low temperature. The upper dashed line labeled  $C$  represents the Langevin capture rate coefficient calculated from Eq. (17) in Eq. (14).

tribute 33% of the total loss rate. The RE rate is so large because survival for the  $1_u$  entrance channel is good, due to the relatively long lifetime of this channel (see Fig. 3). The good agreement between experiment and theory evident in Fig. 10 may be partly fortuitous given the approximations in the theory concerning long-range excitation and the neglect of hyperfine structure. Between 100  $\mu\text{K}$  and 1 mK there is an uncertainty between a factor of 2 and 4 in the rate coefficient due to the ambiguity in the choice of excited-state kinetic energy in calculating the average survival factor. We favor here the choice based on satisfying the local Franck-Condon principle because it leads to agreement with the measured rate. However, we caution that this is a subject that needs to be explored more thoroughly by a more rigorous theory. We are unable to reproduce the rate coefficient quoted in Ref. [22] for the GP theory, which is about a factor of 4 smaller than the experiment. However, the potential and probability parameters used were not given in that reference. Figure 9 shows that the GP expressions should give a rate about twice ours if the same molecular parameters are used in both calculations.

### C. Trap loss for other alkali-metal species

Figure 11 shows our calculated loss rates between 0.1 and 2 mK for a detuning of  $\gamma_A$ , a laser power of 10 mW/cm<sup>2</sup>, and an initial energy choice based on satisfying the local Franck-Condon principle, Eq. (56). Table IV shows the percentage contribution from each mechanism

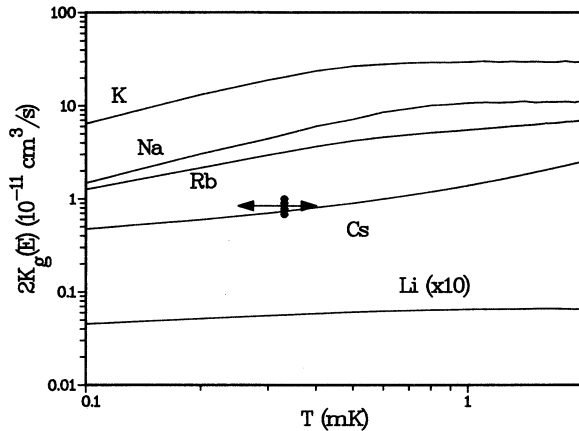


FIG. 11. Calculated trap-loss rate coefficients versus collision energy at a laser power of 10 mW/cm<sup>2</sup>, a detuning of one linewidth, and  $\Delta_{RE}/2k_B = 1$  K. Both FS and RE contributions are included for all five alkali pairs. The rate for Li has been multiplied by 10.

at  $T_D$  for this choice of  $E'(R)$ , as well as the total loss rates for either choice of  $E'(R)$ , Eqs. (55) or (56). The experimental data for Cs are also indicated in Fig. 11. It is evident that there is a wide variation in magnitude and mechanism among the alkali-metal species. We will examine the various cases.

The largest trap-loss rates are calculated for K, Na, and Rb. The reason the coefficient for K is several times larger than that for Na, other factors being equal, is that the  $\lambda^2\phi\tau_A$  factor in Eq. (27) is 3.7 times larger for K than Na at the same power. Table IV shows that the dominant mechanism for the FS process in Na and K (and even for Rb) is Coriolis coupling through the  $2_u$  channel. This dominance of the  $2_u$  channel at low temperature is because of the excellent survival relative to radiative decay. This is where retardation has a very important role to play (see Fig. 3): the  $2_u$  state can be excited at long range but leads to very slow radiative decay as the atoms move closer together. Figure 12 shows the contributions to the integrand for the excitation and survival factor  $I(E, 2_u)$  for Na at 1 mK. This may be contrasted with

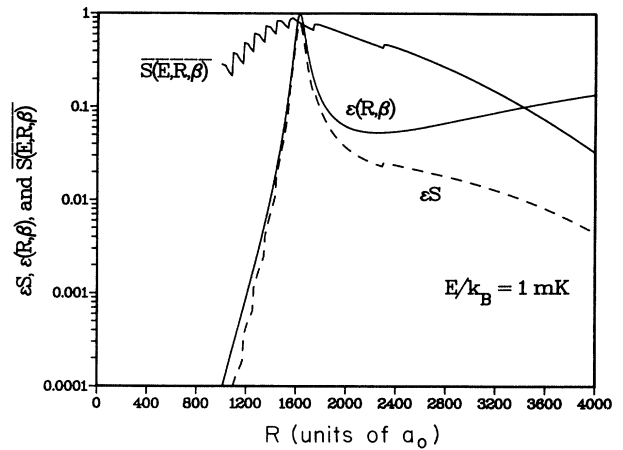


FIG. 12. Absorption and survival factors in the integrand of the  $I(E, \beta)$  function for the  $2_u$  entrance channel for Na<sub>2</sub> for a detuning of one linewidth. The choice of Eq. (55) for the initial kinetic energy was used to calculate the survival factor.

Fig. 6 for Cs. Figure 12 shows  $\epsilon(R, 2_u)$  peaks sharply at the Condon point due to the small radiative decay width. The average survival factor near  $R_C$  is near unity. The dropoff and “oscillations” in  $\bar{S}$  to small  $R$  are due to the same reasons discussed for Cs. Since  $I(E, 2_u) = 0.75$  at 1 mK for Na, there are no significant losses due to excited-state radiative decay, whereas the  $0_u^+$  channel with  $I(E, 0_u^+) = 0.033$  shows major losses. Although the  $2_u$  and  $0_u^+$  channels make comparable contributions to FS collisions for Na and K at room temperature, the  $2_u$  channel is predicted to be completely dominant at ultracold temperature. The FS probability for this channel decreases strongly at low  $T$  because it varies as  $I_{\max}^2$ . Even in Rb where the  $2_u$  FS probability is small, the  $2_u$  channel makes a major contribution at ultracold  $T$ . The RE process is not very significant for Na, K, or Rb.

The species Li is calculated to have a much smaller trap-loss rate than any of the other alkali-metal species. This is because the FS process will not contribute if we assume a trap depth on the order of 1 K because of the small fine-structure interval in Li. The RE probability is

TABLE IV.  $K_{\text{loss}}$  at  $T_D$  with  $\delta = h\gamma_A$ ,  $h\nu\phi = 10$  mW/cm<sup>2</sup>, and  $\Delta_{RE}/2k_B = 1$  K.

| Species | $T_D$ ( $\mu$ K) | % Contribution |                |              | $K_{\text{loss}}$ ( $10^{-11}$ cm <sup>3</sup> /s) |       |
|---------|------------------|----------------|----------------|--------------|--|-------|
|         |                  | RE             | FS ( $0_u^+$ ) | FS ( $2_u$ ) | $G^a$  | $L^b$ |
| Li      | 140              | 100            |                |              | 0.004  | 0.004 |
| Na      | 240              | 5              | 1              | 94           | 2.1  | 3.5   |
| K       | 140              | 5              | 1              | 94           | 6.0  | 8.9   |
| Rb      | 150              | 12             | 30             | 58           | 3.0  | 1.7   |
| Cs      | 130              | 35             | 64             | 1            | 1.8  | 0.5   |

<sup>a</sup>Uses global energy conservation, Eq. (55).

<sup>b</sup>Uses local energy conservation, Eq. (56).

also intrinsically smaller for Li, since the molecular transitions are forbidden for Hund's case-(a) molecular coupling scheme that applies in the region of the trajectory that contributes to RE loss in Li. The slight breakdown in Hund's case-(a) coupling leads to small RE decay rates that scale as  $\Delta E_{\text{RE}}^{-17/6}$  for traps near 1 K (see Sec. III D). The Li rates reported in Fig. 11 and Table IV were calculated using the potentials and decay rates for the  $0_u^+$  and  $1_g$  states found from numerically diagonalizing the Hamiltonian matrices [48–50].

There is very little data to compare with on the other alkali-metal species. Prentiss *et al.* [18] reported a rate coefficient, with an estimated accuracy of only a factor of 5, for a trap-loss process in a Na magneto-optical trap with  $T$  near  $T_D$ . However, the rate coefficient varied only slightly with laser intensity over a range of 5–50 mW/cm<sup>2</sup>, and this experiment has been criticized by Sesko *et al.* [22]. The magnitude of the reported loss rate,  $4 \times 10^{-11}$  cm<sup>3</sup>/s, is in good agreement with our calculated result in Fig. 11 at 10 mW/cm<sup>2</sup>. However, this agreement should not be taken seriously until the experiment is better understood. One complication that could affect comparison of theory and experiment is the density variations and channeling [96,97] that occur on the scale of the wavelength of light. Recall the warning given in Sec. II that the collision is a continuation of the process of laser cooling in which two atoms slowly come together and are no longer cooled independently but are optically pumped as a quasimolecule. Proper comparison of theory and experiment requires averaging over all local conditions in a trap. We have assumed a uniform density distribution and a statistical distribution of states. If these assumptions are violated, the physical mechanisms and FS and RE probabilities we have provided could still be used to make an improved estimate of trap-loss rates.

The GP paper reported an effective  $K^*$  coefficient for Na. We estimate from their Fig. 1 that  $K^*$  is  $2 \times 10^{-11}$  cm<sup>3</sup>/s for  $\delta/h = \gamma_A$ , whereas our  $K_{\text{loss}}$  in Table IV corresponds to a  $K^*$  of  $1.7 \times 10^{-10}$  cm<sup>3</sup>/s. The GP theory misses two critically important effects for trap loss in Na. Their effective state decays far too rapidly, causing their survival factor to be too small. This error is partially compensated by assuming a room-temperature probability for FS, which is far too large at low  $T$  (see Sec. III E and Table III). Using the correct low-temperature average FS probability would cause their rate coefficient to be about an order of magnitude smaller than reported. This demonstrates the necessity of using the correct molecular parameters and mechanisms in order to make valid predictions concerning low-temperature trap-loss rates.

#### D. Role of bound states for large red detunings

We have deliberately kept our analysis of the RE and FS processes as excited-state collisional processes which connect with normal thermal processes as  $T$  is raised. This is appropriate as long as the detuning is comparable to  $\gamma_A$ . But if the detuning of the excitation laser is progressively detuned to the red, the collision switches over to behavior characteristic of ground-state collisions modified by the presence of excited-state rovibronic

bound-state structure. This resonance scattering viewpoint was adopted by Thorsheim, Weiner, and Julienne [98] in describing photoassociation spectroscopy, which should be possible for cold collisions. The “catalysis laser” regime described by Sesko *et al.* [22] occurs in the transition range between the two limits of small and large detuning. If the density of excited bound rovibronic states is large enough, as it will be near the dissociation limit of an attractive  $1/R^3$  potential, then the quantization of the excited-state levels can be ignored and the spectrum approximated as a continuum. This is the quasistatic continuum picture used by Gallagher and Pritchard for red detuning. The criterion for using such a picture is that the level spacing be smaller than the level width. This picture fails when the levels are resolved, that is, when the vibrational or rotational frequency is larger than the decay rate, or

$$\Delta G_{v,\beta}/h > \tau_\beta \quad (58)$$

for vibrational levels and

$$2B_{v,\beta}^l/h > \tau_\beta \quad (59)$$

for rotational levels, where  $\Delta G_v$  and  $B_v$  are the usual vibrational spacing and rotational constant in spectroscopic notation. Here  $\tau_\beta$  is the lifetime of state  $\beta$  due to all decay processes, radiative and predissociation. For example, the  $0_u^+$  state will be broadened by predissociation decay into the  $0_u^+$  or  $1_u$  states which connect with the  $^2P_{1/2}$  asymptotic atom. The predissociation decay rate can be written as

$$\tau_\beta^{-1} = (\Delta G_{v,\beta}/h)P(E_v, l, \beta), \quad (60)$$

where  $P$  is the probability of the FS process during a single vibrational cycle of state  $\beta$  [99]. Using generalized multichannel quantum-defect theory [23,99], the probabilities  $P$  in Table III may be extrapolated across threshold to apply to the bound states below threshold. The resulting predissociation rates are typically much larger than the radiative decay rate. This fact suggests an experimental test of the FS changing mechanism and probability. If the rovibronic levels are well separated, and the  $^2P_{1/2}$  product is detected as a function of excitation wavelength tuned near resonance with a bound level, then the resulting excitation spectrum maps out the line shape and width of the level. This gives a direct spectroscopic measure of the FS contribution to the probability. Such an experiment may be feasible using either laser spectroscopy or photoassociation spectroscopy of cold trapped atoms [98].

It is simple to work out the detuning ranges in which rotationally and vibrationally resolved spectra could be observed. Using the well-known expression for the vibrational spacing for the levels in a  $1/R^3$  potential [100,101], vibrational resolution according to (58) is achieved when

$$\delta > [2\pi\mu\Gamma(\frac{5}{6})^2/9\Gamma(\frac{4}{3})^2]^{3/5}C(\beta)^{2/5}/\tau_\beta^{6/5}. \quad (61)$$

This is only on the order of a few hundred MHz if the broadening is due to radiative processes. Using (60) in (58) shows that resolution is always achieved relative to

predissociation if  $P \ll 1$ . Achieving rotational resolution requires larger detunings. However, in photoassociation spectroscopy, the ground-state centrifugal potential limits the number of upper rotational levels that can be excited. Only partial waves with  $l < l_\delta$  contribute if

$$\delta > \left[ \frac{2\mu\epsilon}{\hbar^2 l_\delta (l_\delta + 1)} \right]^{3/2} C(\beta). \quad (62)$$

Setting  $l_\delta = 1$  sets the criterion for only  $s$  waves contributing to the spectrum. In this limit, the spectrum will be rotationally and vibrationally resolved. This criterion is only 0.6 GHz for the  $1_u$  state of  $\text{Na}_2$  but increases to 47 GHz ( $1.6 \text{ cm}^{-1}$ ) for the  $0_u^+$  state of  $\text{Cs}_2$ .

## V. CONCLUSION

We have presented a theory that describes the temperature dependence of the rate coefficients for collision of ground and excited states of like alkali-metal atoms. We have identified the physical mechanisms of fine-structure-changing collisions at both normal and ultracold temperatures. Quantum scattering calculations verify the basic qualitative picture of these collisions worked out by Dashevskaya [71]. Except for Cs, the room-temperature rates tend to be about a factor of 2 smaller than experimental values. We were able to obtain agreement with measured rates for Cs at 300 K and 300  $\mu\text{K}$  by using a matrix element estimated from low resolution spectroscopy. An accurate determination of this matrix element is needed for both Cs and Rb. We hope our work stimulates interest in new and improved measurements of alkali-metal FS collisions as a function of temperature. It would be especially interesting if the region from 10 mK to 1 K could be explored where switching occurs between “normal” collisions and ultracold collisions. If feasible, beam experiments with optical control of collision energy would be highly desirable, especially if they could be used to study atomic alignment effects on the FS rate coefficient.

Low-temperature excited-state collisions are unique in that the excited state is only produced when the two atoms are close enough together that they absorb as a quasimolecule. For near-resonant light the excitation distance is so large that retardation corrections to the quasimolecular radiative transition rates have dramatic consequences for the collision dynamics, at least for the species Na, K, and Rb. In order to develop a manageable theory, both we and GP had to make many simplifying assumptions about the long-range excitation process. It is important to develop a proper quantum-mechanical treatment of the cold collision in a radiation field, including excited-state decay, in order to examine the role of the following factors: (1) hyperfine structure and its role in quasimolecular optical pumping, (2) light shift and saturation effects on the excitation process, and (3) nonadiabatic channel mixing associated with the transformation from the laboratory to rotating molecule angular momentum quantization frames as the atoms come together.

In view of the many approximations in our theory, it is remarkable that such good agreement was found with the

measured rate of the Cs trap-loss experiment. We believe that it is important to carry out experiments on other alkali-metal species to help clarify our understanding of the trap-loss process. One interesting aspect of this is to look for isotope effects. A good example might be  $^{85}\text{Rb}$  and  $^{87}\text{Rb}$ . These isotopes have different hyperfine structures and may show different trap-loss rates if the hyperfine structure plays a significant role. Our simple theory neglects hyperfine structure and predicts the same loss rate for both isotopes. Measured deviations from this prediction could provide guidance for developing an improved theory. We also hope that it will be possible to do experiments on bound-state spectroscopy near the  $^2P_{3/2} + ^2S_{1/2}$  dissociation limit. This could be done in high resolution with an ultracold photoassociation experiment and could yield much information about the FS probabilities. A recent laser spectroscopy experiment [102] on the  $\text{H}_2$  molecule very close to the  $n=2$  dissociation limit revealed unexpected perturbations in the molecular levels, probably associated with hyperfine structure, and showed that the spectroscopy of long-range molecular states is a feasible and challenging opportunity. In fact, the possibility of carrying out  $\text{H}_2$  spectroscopy near  $n=2$  using photoassociation spectroscopy of cold trapped spin-polarized H atoms is a subject which we intend to explore.

## ACKNOWLEDGMENTS

This work was supported in part by the U.S. Air Force Office of Scientific Research. One of us (P.S.J.) wishes to thank the University of Paris for providing support for part of this work.

## APPENDIX A: PAIR DISTRIBUTION FUNCTION

The derivation of the pair distribution function, Eq. (21), follows well-established methods [103–106]. We provide a brief outline, since we did not find an explicit derivation readily available in the literature. The classical partition function of two distinguishable particles due to their relative motion is

$$Q = h^{-3} \int \int \int \int \int \int e^{-H/k_B T} dR d\theta d\phi dp_R dp_\theta dp_\phi, \quad (A1)$$

where

$$H = p_R^2 + (p_\theta^2 + p_\phi^2 / \sin^2\theta) / (2\mu R^2) + V(R). \quad (A2)$$

By making the transformation of variables

$$E = H, \quad (A3a)$$

$$q = (p_\theta^2 + p_\phi^2 / \sin^2\theta) / (2\mu), \quad (A3b)$$

$$\gamma = \tan^{-1}(p_\theta \sin \theta / p_\phi), \quad (\text{A3c})$$

the Jacobian gives

$$dp_R dp_\theta dp_\phi$$

$$= 2 \frac{\mu^{3/2}}{\sqrt{2}} \sin \theta [E - q/R^2 - V(R)]^{-1/2} dE dq d\gamma, \quad (\text{A4})$$

where the ranges are

$$-\infty < p_R < +\infty, \quad E \geq V(R)$$

$$-\infty < p_\theta < +\infty, \quad 0 \leq q \leq R^2[E - V(R)] \quad (\text{A5})$$

$$-\infty < p_\phi < +\infty, \quad -\pi \leq \phi \leq \pi.$$

Stogryn and Hirshfelder [106] pointed out that the existence of + and - momenta  $p_R$ , that is, approaching and separating atoms, required the introduction of the factor of 2 in the phase volume, Eq. (A4). After integrating over  $\theta$ ,  $\phi$ , and  $\gamma$  to get  $8\pi^2$ , the classical partition function becomes

$$Q = \frac{(2\mu)^{1/2}}{h} \int_0^\infty dR \int_{V(R)}^\infty dE (2\mu/\hbar^2) \int_0^{R^2[E-V(R)]} dq \frac{e^{-E/k_B T}}{[E - q/R^2 - V(R)]^{1/2}}. \quad (\text{A6})$$

If the integration over  $q$  and  $E$  is carried out, using

$$\int_0^{R^2[E-V(R)]} dq \frac{1}{[E - q/R^2 - V(R)]^{1/2}} = 2R^2[E - V(R)]^{1/2}, \quad (\text{A7})$$

we get the usual result for the partition function:

$$Q = Q_{\text{tr}} \int_0^{R_0} dR 4\pi R^2 e^{-V(R)/k_B T}, \quad (\text{A8})$$

where  $Q_{\text{tr}} = (2\pi\mu k_B T/h^2)^{3/2}$  is the translational partition function per unit volume. For an ideal gas  $V(R) = 0$ , and  $Q = Q_0 = Q_{\text{tr}} V$ , where  $V$  is the volume. These results are standard, and show that we have the correct integration after making the transformation of variables. The integration is over *both* approaching *and* separating atoms.

If  $N_A$  and  $N_B$  are the respective numbers of nonidentical species  $A$  and  $B$  in volume  $V$ , the total number of

pairs in volume  $V$  is

$$N = N_A N_B Q / Q_0, \quad (\text{A9})$$

and the number of pairs per unit volume is

$$n = N/V = (N_A/V)(N_B/V)Q/Q_{\text{tr}} = n_A n_B Q/Q_{\text{tr}}. \quad (\text{A10})$$

Using the classical-quantum correspondence,

$$q \leftrightarrow \hbar^2 l(l+1)/2\mu, \quad (\text{A11a})$$

$$dq \leftrightarrow (\hbar^2/2\mu)(2l+1), \quad (\text{A11b})$$

$$(2\mu/\hbar^2) \int_0^{R^2[E-V(R)]} dq \leftrightarrow \sum_{l=0}^{l_{\text{max}}} (2l+1). \quad (\text{A11c})$$

Equations (A6) and (A10) show that the density of pairs in  $dR$  and  $dE$  with  $dl = 2\mu dq/\hbar^2 = 1$  is

$$dn(R, E, l) = n_A n_B Q_{\text{tr}}^{-1} \frac{(2\mu)^{1/2}}{h} \frac{e^{-E/k_B T}}{[E - q/R^2 - V(R)]^{1/2}} dR dE (2\mu/\hbar^2) dq \quad (\text{A12a})$$

$$= n_A n_B \frac{2}{h Q_{\text{tr}}} \frac{(2l+1)}{v(R, E, l)} e^{-E/k_B T} dR dE. \quad (\text{A12b})$$

The pair distribution in Eq. (21) follows from (A12b) upon noting two facts. First, half of the pairs are approaching and half are separating. The number of approaching pairs that can react is therefore half of (A12b). Second, if the species  $A$  and  $B$  are identical,  $n_A = n_B = n$ ,

an additional symmetry factor of  $\frac{1}{2}$  must be introduced in order not to count phase space twice for the identical particles, i.e., replace  $n_A n_B$  by  $n^2/2$ . By writing  $2dR/v(R, E, l) = dt$ , where  $dt$  is the classical time spent in  $dR$ , the physical meaning of the  $l$ -dependent velocity

in the denominator of (A12b) may be more apparent. Equation (A12b) is the equilibrium constant for occupying one quantum of phase space, if  $dt dE$  is set equal to  $h$ .

#### APPENDIX B: MOLECULAR ABSORPTION COEFFICIENT

Taking the standard formulas for atomic absorption from Mitchell and Zemansky [107], the integrated photo-absorption is

$$\int \sigma(\nu) d\nu = \frac{\lambda^2 g'}{8\pi g'' \tau'} \quad (\text{B1})$$

where  $\nu$  is in hertz and the absorption is from a lower state with degeneracy  $g''$  to an upper state with degeneracy  $g'$ . The upper level decays to the lower with lifetime  $\tau'$ . Equation (B1) shows  $\sigma(\nu)$  may be written as

$$\sigma(\nu) = \frac{\lambda^2 g'}{8\pi g'' \tau'} g(\delta) \quad (\text{B2})$$

where  $g(\delta)$  is the normalized line-shape function for detuning  $\delta$  in hertz:

$$\int_{-\infty}^{+\infty} g(\delta) d\delta = 1 \quad (\text{B3})$$

For natural broadening

$$g(\delta)/h = \frac{h\gamma'}{2\pi \delta^2 + (h\gamma'/2)^2} \quad (\text{B4})$$

where  $\gamma' = (2\pi\tau')^{-1}$  is the natural linewidth. It follows from (B2) and (B4) that the peak cross section

$$\sigma(0) = \frac{\lambda^2 g'}{2\pi g''} \quad (\text{B5})$$

is independent of  $\tau'$  and  $\gamma'$ , and  $\sigma(\nu)$  can also be written in terms of its peak value

$$\begin{aligned} \sigma(\nu) &= \frac{\lambda^2 g'}{2\pi g''} [1 + (2\delta/h\gamma')^2]^{-1} \\ &= \sigma(0)\epsilon(\delta, \gamma') \quad (\text{B6}) \end{aligned}$$

Equation (B6) immediately shows that the absorption cross section for a quasimolecule with  $g'' = g_1^2$  degenerate ground-state components absorbing to a single upper-state component  $\beta(g' = 1)$ , which decays back to the  $g_1^2$  ground-state components at rate  $\tau_\beta^{-1}$ , is given by Eq. (22).

- 
- [1] S. V. Andreev, V. I. Balykin, V. S. Letokhov, and V. G. Minogin, Pis'ma Zh. Eksp. Teor. Fiz. **34**, 463 (1981) [JETP Lett. **34**, 442 (1981)].
- [2] J. V. Prodan, A. Migdall, W. D. Phillips, I. So, H. J. Metcalf, and J. Dalibard, Phys. Rev. Lett. **54**, 992 (1985).
- [3] W. Ertmer, R. Blatt, J. L. Hall, and M. Zhu, Phys. Rev. Lett. **54**, 996 (1985).
- [4] A. L. Migdall, J. V. Prodan, W. D. Phillips, T. H. Bergeman, and H. J. Metcalf, Phys. Rev. Lett. **54**, 2596 (1985).
- [5] S. Chu, L. Holberg, J. E. Bjorkholm, A. Cable, and A. Ashkin, Phys. Rev. Lett. **55**, 49 (1985).
- [6] S. Chu, J. E. Bjorkholm, A. Ashkin, and A. Cable, Phys. Rev. Lett. **57**, 314 (1986).
- [7] E. L. Raab, M. Prentiss, A. Cable, S. Chu, and D. E. Pritchard, Phys. Rev. Lett. **59**, 2631 (1987).
- [8] V. S. Bagnato, G. P. Lafyatis, A. G. Martin, E. L. Raab, R. N. Ahmed-Bitar, and D. E. Pritchard, Phys. Rev. Lett. **58**, 2194 (1987).
- [9] R. N. Watts and C. E. Wieman, Opt. Lett. **11**, 291 (1986).
- [10] D. Sesko, C. Fan, and C. E. Wieman, J. Opt. Soc. Am. B **5**, 1225 (1988).
- [11] P. D. Lett, R. N. Watts, C. I. Westbrook, W. D. Phillips, P. L. Gould, and H. J. Metcalf, Phys. Rev. Lett. **61**, 169 (1988); P. D. Lett, W. D. Phillips, S. L. Rolston, C. E. Tanner, R. N. Watts, and C. I. Westbrook, J. Opt. Soc. Am. B **6**, 2084 (1989).
- [12] D. S. Weiss, E. Riis, Y. Shevy, P. J. Ungar, and S. Chu, J. Opt. Soc. Am. B **6**, 2072 (1989).
- [13] F. Shimizu, K. Shimizu, and H. Takuma, Phys. Rev. A **39**, 2758 (1989).
- [14] C. Salomon, J. Dalibard, W. D. Phillips, A. Clairon, and S. Guellati, Europhys. Lett. **12**, 683 (1990).
- [15] C. Monroe, W. Swann, H. Robinson, and C. Wieman, Phys. Rev. Lett. **65**, 1571 (1990).
- [16] J. Vigue, Phys. Rev. A **34**, 4476 (1986).
- [17] D. Pritchard, in *Electronic and Atomic Collisions*, edited by D. C. Lorents, W. E. Meyerhof, and J. R. Peterson (North-Holland, Amsterdam, 1986), p. 593.
- [18] M. Prentiss, A. Cable, J. E. Bjorkholm, S. Chu, E. L. Raab, and D. E. Pritchard, Opt. Lett. **13**, 452 (1988).
- [19] P. S. Julienne, S. H. Pan, H. R. Thorsheim, and J. Weiner, in *Advances in Laser Science*, Proceedings of the Third International Laser Science Conference, Atlantic City, New Jersey, 1987, edited by A. C. Tam, J. L. Gole, and W. C. Stwalley, AIP Conf. Proc. No. 172 (AIP, New York, 1988), Vol. 3, p. 308.
- [20] P. L. Gould, P. D. Lett, P. S. Julienne, W. D. Phillips, H. R. Thorsheim, and J. Weiner, Phys. Rev. Lett. **60**, 788 (1988).
- [21] A. Gallagher and D. E. Pritchard, Phys. Rev. Lett. **63**, 957 (1989).
- [22] D. Sesko, T. Walker, C. Monroe, A. Gallagher, and C. Wieman, Phys. Rev. Lett. **63**, 961 (1989).
- [23] P. S. Julienne and F. H. Mies, J. Opt. Soc. Am. B **6**, 2257 (1989).
- [24] P. S. Julienne, Phys. Rev. Lett. **61**, 698 (1988).
- [25] P. L. Gould, P. D. Lett, R. N. Watts, C. I. Westbrook, P. S. Julienne, W. D. Phillips, H. R. Thorsheim, and J. Weiner, in *Atomic Physics II*, edited by S. Haroche, J. C. Gay, and G. Grynberg (World Scientific, Singapore, 1989).
- [26] H. Thorsheim, Ph.D. thesis, University of Maryland, 1989.
- [27] J. Weiner, J. Opt. Soc. Am. B **6**, 2270 (1989).
- [28] J. Dalibard and C. Cohen-Tannoudji, J. Opt. Soc. Am. B **6**, 2023 (1989).
- [29] P. J. Ungar, D. S. Weiss, E. Riis, and S. Chu, J. Opt. Soc. Am. B **6**, 2058 (1989).
- [30] E. Riis, D. S. Weiss, K. A. Moler, and S. Chu, Phys. Rev. Lett. **64**, 1658 (1990).
- [31] M. Trippenbach and J. Cooper, in *Coherence and Quan-*

- tum Optics VI*, edited by J. H. Eberly *et al.* (Plenum, New York, 1990), p. 1165.
- [32] A. Ben-Reuven, in *Spectral Line Shapes*, edited by L. Frommhold and J. Keto (AIP, New York, 1990), Vol. 6, p. 206.
- [33] A. Smith and K. Burnett, *J. Opt. Soc. Am. B* **8**, 1592 (1991).
- [34] In the correct quantum-mechanical treatment of homonuclear symmetry, the degeneracy factor is only 8, but every other partial wave is missing from the sum over  $l$ , if nuclear spin  $I=0$ , and is weighted by a nuclear spin factor having average value  $\frac{1}{2}$  if  $I \neq 0$ . See Manders *et al.*, *Phys. Rev. A* **39**, 5021 (1989). Our choice is equivalent to that of Ref. [48].
- [35] R. S. Mulliken, *Phys. Rev.* **120**, 1674 (1960).
- [36] R. R. McClone and E. A. Power, *Proc. R. Soc. London, Ser. A* **286**, 573 (1965); *Mathematika* **11**, 91 (1969).
- [37] M. J. Stephen, *J. Chem. Phys.* **40**, 669 (1964).
- [38] E. A. Power, *J. Chem. Phys.* **46**, 4297 (1967).
- [39] W. J. Meath, *J. Chem. Phys.* **45**, 4519 (1966).
- [40] W. J. Meath, *J. Chem. Phys.* **48**, 227 (1968).
- [41] D. K. Watson, C. J. Cerjan, S. Guberman, and A. Dalgarno, *Chem. Phys. Lett.* **50**, 181 (1977).
- [42] D. D. Konowalow, M. E. Rosenkrantz, and M. L. Olson, *J. Chem. Phys.* **72**, 2612 (1980).
- [43] D. D. Konowalow and M. E. Rosenkrantz, *J. Phys. Chem.* **86**, 1099 (1982).
- [44] D. D. Konowalow and M. E. Rosenkrantz, in *Metal Bonding and Interactions in High Temperature Systems*, edited by J. L. Gole and W. C. Stwalley (American Chemical Society, New York, 1982).
- [45] G. H. Jeung, F. S. Spiegelmann, J. P. Daudey, and J. P. Malrieu, *J. Phys. B* **16**, 2659 (1983).
- [46] G. H. Jeung and A. J. Ross, *J. Phys. B* **21**, 1473 (1988).
- [47] M. Krauss and W. J. Stevens, *J. Chem. Phys.* **93**, 4236 (1990).
- [48] E. I. Dashevskaya, A. I. Voronin, and E. E. Nikitin, *Can. J. Phys.* **47**, 1237 (1969).
- [49] M. Movre and G. Pichler, *J. Phys. B* **10**, 263 (1977).
- [50] B. Bussery and M. Aubert-Frecon, *J. Chem. Phys.* **82**, 3224 (1985).
- [51] R. N. Zare, A. L. Schmeltekopf, W. J. Harrop, and D. L. Albritton, *J. Mol. Spectrosc.* **46**, 37 (1973).
- [52] J. M. Brown, J. T. Hougen, K.-P. Huber, J. W. C. Johns, I. Kopp, H. Lefebvre-Brion, A. J. Merer, D. A. Ramsay, J. Rostas, and R. N. Zare, *J. Mol. Spectrosc.* **55**, 500 (1975).
- [53] S. J. Singer, K. F. Freed, and Y. B. Band, *J. Chem. Phys.* **79**, 6060 (1983).
- [54] W. L. Wiese, M. W. Smith, and B. M. Glennon, *Atomic Transition Probabilities*, Natl. Bur. Stand. Ref. Data Ser., Natl. Bur. Stand. (U.S.) Circ. No. 4 (U.S. GPO, Washington, DC, 1966), Vol. 1.
- [55] J. K. Link, *J. Opt. Soc. Am.* **56**, 1195 (1966).
- [56] R. W. Schmieder, A. Lurio, W. Happer, and A. Khadjavi, *Phys. Rev. A* **2**, 1216 (1970).
- [57] J. C. Weisheit, *Phys. Rev. A* **5**, 1621 (1972).
- [58] R. W. Schmieder, A. Lurio, and W. Happer, *Phys. Rev.* **173**, 76 (1968).
- [59] D. Zimmermann, *Z. Phys. A* **275**, 5 (1975).
- [60] S. Svanberg, *Phys. Scr.* **4**, 269 (1971).
- [61] S. Svanberg and S. Rydberg, *Z. Phys.* **227**, 216 (1969).
- [62] M. Movre and G. Pichler, *J. Phys. B* **13**, 697 (1980).
- [63] W. C. Stwalley, Y.-H. Uang, and G. Pichler, *Phys. Rev. Lett.* **41**, 1164 (1978).
- [64] B. Bussery and M. Aubert-Frecon, *J. Mol. Spectrosc.* **113**, 21 (1985).
- [65] M. Czajkowski and L. Krause, *Can. J. Phys.* **43**, 1259 (1965).
- [66] A. G. A. Rae and L. Krause, *Can. J. Phys.* **43**, 1574 (1965).
- [67] G. D. Chapman and L. Krause, *Can. J. Phys.* **44**, 753 (1966).
- [68] J. Pitre and L. Krause, *Can. J. Phys.* **46**, 125 (1968).
- [69] M. Stupansky and L. Krause, *Can. J. Phys.* **47**, 1269 (1969).
- [70] L. Krause, *Adv. Chem. Phys.* **28**, 267 (1975).
- [71] E. I. Dashevskaya, *Opt. Spektrosk.* **46**, 423 (1979) [*Opt. Spectrosc.* **46**, 236 (1979)].
- [72] E. E. Nikitin, *Adv. Chem. Phys.* **28**, 317 (1975).
- [73] D. Feldman and R. N. Zare, *Chem. Phys.* **15**, 415 (1976).
- [74] V. B. Grushevskii, S. M. Papernov, and M. L. Yanson, *Opt. Spektrosk.* **44**, 809 (1978) [*Opt. Spectrosc. (USSR)* **44**, 475 (1978)].
- [75] E. K. Kraulinya and M. L. Yanson, *Opt. Spektrosk.* **46**, 1112 (1979) [*Opt. Spectrosc. (USSR)* **46**, 629 (1979)].
- [76] E. J. Bredford and E. Engelke, *Chem. Phys. Lett.* **75**, 132 (1980).
- [77] E. W. Rothe, U. Krause, and R. Duren, *J. Chem. Phys.* **72**, 5145 (1980).
- [78] C. B. Collins, F. W. Lee, J. A. Anderson, P. A. Vicharelli, D. Popescu, and I. Popescu, *J. Chem. Phys.* **74**, 1067 (1981).
- [79] M. L. Janson and S. M. Papernov, *J. Phys. B* **15**, 4175 (1982).
- [80] G. Gerber and R. Moller, *Phys. Rev. Lett.* **55**, 814 (1985).
- [81] V. Zafropulos, P. D. Kleiber, K. M. Sando, X. Zeng, A. M. Lyyra, and W. C. Stwalley, *Phys. Rev. Lett.* **61**, 1485 (1988); V. Zafropulos, Ph.D. thesis, University of Iowa, 1988.
- [82] R. L. Dubs and P. S. Julienne, *J. Chem. Phys.* (to be published).
- [83] W. S. Struve, S. J. Singer, and K. F. Freed, *Chem. Phys. Lett.* **110**, 588 (1984).
- [84] C. Effantin, O. Babaky, K. Hussein, J. d'Incan, and R. F. Barrow, *J. Phys. B* **18**, 4077 (1985).
- [85] X. Xie and R. W. Field, *Chem. Phys.* **99**, 337 (1985).
- [86] A. J. Ross, P. Crozet, C. Effantin, J. d'Incan, and R. F. Barrow, *J. Phys. B* **20**, 6225 (1987).
- [87] M. J. O'Callahan, A. Gallagher, and T. Holstein, *Phys. Rev. A* **32**, 2754 (1985).
- [88] P. S. Julienne, *J. Appl. Phys.* **48**, 4140 (1977).
- [89] P. S. Julienne, *J. Chem. Phys.* **68**, 32 (1978).
- [90] R. E. M. Hedges, D. L. Drummond, and A. Gallagher, *Phys. Rev. A* **6**, 1519 (1972).
- [91] P. S. Herman and K. M. Sando, *J. Chem. Phys.* **68**, 1153 (1978).
- [92] H. Orth, H. Ackerman, and E. W. Otten, *Z. Phys. A* **273**, 221 (1975).
- [93] P. S. Julienne, *Phys. Rev. A* **26**, 3299 (1982).
- [94] F. H. Mies, P. S. Julienne, Y. B. Band, and S. J. Singer, *J. Phys. B* **19**, 3249 (1986).
- [95] T. Walker, D. Sesko, and C. Wieman, *Phys. Rev. Lett.* **64**, 408 (1990).
- [96] N. P. Bigelow and M. G. Prentiss, *Phys. Rev. Lett.* **65**, 29 (1990).
- [97] C. I. Westbrook, R. N. Watts, C. E. Tanner, S. L. Rolston, W. D. Phillips, P. D. Lett, and P. L. Gould, *Phys. Rev. Lett.* **65**, 33 (1990).
- [98] H. R. Thorsheim, J. Weiner, and P. S. Julienne, *Phys.*

- Rev. Lett. **58**, 2420 (1987).
- [99] P. S. Julienne and F. H. Mies, in *Electronic and Atomic Collisions*, edited by D. C. Lorents, W. E. Meyerhof, and J. R. Petersen (North-Holland, Amsterdam, 1986), p. 725.
- [100] R. J. LeRoy and R. B. Bernstein, *J. Chem. Phys.* **52**, 3869 (1970).
- [101] W. C. Stwalley, *Chem. Phys. Lett.* **6**, 241 (1970).
- [102] E. McCormack and E. E. Eyler, *Phys. Rev. Lett.* **66**, 1042 (1991); E. McCormack, Ph.D. thesis, Yale University, 1990.
- [103] T. L. Hill, *Statistical Mechanics* (McGraw-Hill, New York, 1956).
- [104] T. L. Hill, *J. Chem. Phys.* **23**, 617 (1955).
- [105] D. E. Stogryn and J. O. Hirshfelder, *J. Chem. Phys.* **31**, 1531 (1959).
- [106] D. E. Stogryn and J. O. Hirshfelder, *J. Chem. Phys.* **33**, 942 (1960).
- [107] A. C. G. Mitchell and M. W. Zemansky, *Resonance Radiation and Excited Atoms* (Cambridge University Press, London, 1971), p. 96.